Tailoring physico-mechanical and antimicrobial/antioxidant properties of biopolymeric films by cinnamaldehyde-loaded chitosan nanoparticles and their application in packaging of fresh rainbow trout fillets

Seyed Fakhreddin Hosseini[a,*], Jaber Ghaderi[a], M. Carmen Gómez-Guillén[b]

[a] *Department of Seafood Processing, Faculty of Marine Sciences, Tarbiat Modares University, P.O. Box 46414-356, Noor, Iran*

[b] *Instituto de Ciencia y Tecnología de Alimentos y Nutrición (ICTAN, CSIC), Calle José Antonio Novais, 10, 28040 Madrid, Spain*

[*]**Corresponding author:** Tel: +98 1144999000-3 Fax: +98 1144553499 E-mail: hosseinisf@modares.ac.ir (S. F. Hosseini).

Abstract

In this study, cinnamaldehyde (CIN)-loaded chitosan nanoparticles (CCNPs) were fabricated and embedded into chitosan/poly(vinyl alcohol)/fish gelatin (CPF) ternary matrices to improve the physico-mechanical and biofunctional performances of the films. The particle size and ζ-potential values of the CCNPs were 370.3 nm and +32.2 mV, respectively. SEM images revealed that the CCNPs were homogeneously dispersed in the CPF ternary film matrices, thereby filling void spaces in the composite matrix, and significantly improving the bionanocomposite films tensile properties (from 28.33 ± 2.17 MPa to 33.0 ± 1.28 MPa) ($p < 0.05$). However, the water barrier properties and water contact angle of the CPF films were not significantly influenced by the nanofiller embedding. Although the incorporation of the NPs decreased the light transmittance of the films, it provided the CPF-CCNPs nanocomposite films with excellent UV-barrier properties. ATR/FT-IR spectroscopy and X-ray diffraction analysis demonstrated the formation of hydrogen bonds between the NPs and polymer molecules. TGA and DSC studies revealed that CPF-CCNPs nanocomposite films presented better thermal stability than the neat CPF film. AFM imaging also indicated a re-organization of the surface of the nanocomposite films due to the incorporation of the NPs. Release studies suggested that the CPF-CCNPs bionanocomposite film exhibited sustained release behavior of CIN. Likewise, the bioactive nanocomposites displayed antibacterial activity against food-borne pathogens such as Gram-positive (*Staphylococcus aureus* and *Listeria monocytogenes*) and Gram-negative bacteria (*Escherichia coli* and *Salmonella enteritidis*). The bionanocomposite films exhibited *in vitro* DPPH radical scavenging activity (~16.4%) and ferric reducing power at the maximum CIN loading concentration. Additionally, analysis of storage quality indices (pH, TBARS values, color, and microbiological analyses) revealed the shelf-life of rainbow trout fillets wrapped in CPF-CCNPs0.25 was extended to 12 days.

Keywords: Bionanocomposite films; Chitosan nanoparticles; Cinnamaldehyde; Films characterization; Antimicrobial/antioxidant properties; Fillet preservation

1. Introduction

Recently, the development of new antimicrobial/antioxidant biopackaging materials to extend the shelf-life of foods has received much attention in the food industry. Active packaging is field of growing interest given its duality, both as a barrier against external detrimental factors, and because of their active role in the preservation and quality of food (Vilela et al., 2018). Food-grade biopolymers such as proteins (*e.g.,* fish gelatin, FG) and polysaccharides (*e.g.,* chitosan, CH) have been successfully included in packaging films due to the unique functional properties of such materials *e.g.,* flexibility, transparency, and superior barrier properties against oxygen and UV light (de la Caba et al., 2019; Hosseini & Gómez-Guillén, 2018). Nevertheless, these materials present several problems, *e.g.,* low mechanical strength, poor stability against moisture, and poor water barrier properties, which limit their marketability (Hosseini, Rezaei, Zandi, & Farahmandghavi, 2015a). Blending compatible/miscible biopolymers with synthetic polymers could also modify the properties of the resulting biomaterial in an easy, economical, and nature-friendly procedure. Poly(vinyl alcohol) (PVA) is an attractive synthetic polymer suitable for mixing with biopolymers to improve the functional characteristics because of its interesting physical properties, which arise from the presence of O-H groups and the hydrogen bond formation (Bonilla, Fortunati, Atarés, Chiralt, & Kenny, 2014). In addition, it is easily soluble in water, biodegradable, and it has excellent film-forming and good mechanical properties (Giteru, Ali, & Oeya, 2019). In a previous work, films composed of a blend of CH/PVA/FG in different ratios were developed, and the effects of these ratios on the most relevant characteristics of the films were obtained. According to the results, there was an optimal level of interaction among the three polymers, where FG was the inferior phase in the film system (*i.e.,* 40CH/40PVA/20FG mass

ratio) and the properties of the film were favorable (Ghaderi, Hosseini, Keyvani, & Gómez-Guillén, 2019).

Despite the numerous merits and unique properties of these biodegradable polymers, the greater use of biopolymers as compared with synthetic ones is limited due to their weak mechanical and poor barrier attributes, processing difficulties, and their elevated cost (de la Caba et al., 2019). To overcome the shortcomings of biopolymeric films, a new class of materials, namely bionanocomposites (a biopolymer matrix reinforced with nanoparticles (NPs) mostly in low fractions (1-10%, in mass)), has led to significant improvements in physico-mechanical and thermal attributes as compared with pristine biopolymers or conventional micro- or macroscale composites (Rhim, Park, & Ha, 2013). These improvements can lead to lower weight packages, as less material is required to get the same or even better barrier properties; this, in turn, can lead to reduce packaging costs with less packaging waste. Moreover, NPs may serve as means of interaction between food and the environment and can therefore play a dynamic role in food preservation and protection (active and intelligent packaging) (Hosseini & Gómez-Guillén, 2018). The incorporation of NPs in biopolymers can improve the properties of packaging materials by enhancing their antimicrobial activity, thus preventing foodborne pathogens (Al-Tayyar, Youssef, & Al-hindi, 2020a). Among various NPs, chitosan nanoparticles (CHNPs) obtained through the ionotropic gelation of a CH polycation and a sodium tripolyphosphate (TPP) polyanion (Hosseini, Ramezanzade, & McClements, 2021), which possess excellent physico-chemical properties, bioactivity, are environmentally friendly, and are considered as an attractive reinforcement filler for edible films and/or food packaging (Wu et al., 2019). Nonetheless, the antibacterial activity of CHNPs is limited due to its low polarity, which makes them diffuse slowly from the films to the agar plates (Hosseini, Rezaei, Zandi, & Farahmandghavi, 2016).

89 An emerging field of interest in reference to bioactive packaging studies the incorporation of plant-
90 derived extracts/essential oils that show high efficacy in suppressing the growth of microorganisms
91 and have been used as antimicrobial additives in the active packaging of foods such as cheese,
92 fish, meat, fruits and vegetables (Vilela et al., 2018; Uranga, Etxabide, Guerrero, & de la Caba,
93 2018). Cinnamaldehyde (CIN), a polyphenolic compound found in the essential oil of cinnamon
94 (*Cinnamomum verum*) (60-75% of the total oil), has been considered as natural preservative due
95 to its positive effects against a broad spectrum of pathogenic microorganisms *via* the inhibition of
96 ATPases, cell wall biosynthesis, and alteration of membrane structure and integrity (Chen et al.,
97 2016; Shreaz et al., 2016; Wu, Sun et al., 2019). However, essential oils or their volatile
98 compounds are thermally/oxygen-sensitive and may lose their activity during typical processing
99 methods used for polymeric materials; also, the release rate of bioactive substances directly added
100 to the film is difficult to control, resulting in limited effectiveness (Kuai, Liu, Ma, Goff, & Zhong,
101 2020). Therefore, to reduce losses of bioactivities during film formation or packaging structure
102 development, effective encapsulation technology is urgent (Hosseini, Nahvi, & Zandi, 2019).
103 Nanoencapsulation of bioactive compounds before incorporation into the biopolymeric matrices
104 is one of the convincing technologies to maintain the slow release of bioactives from
105 antimicrobial/antioxidant packaging materials (Cui, Surendhiran, Li, & Lin, 2020).
106 Rainbow trout (*Oncorhynchus mykiss*) with abundant nutrients like protein and ω-3 series of
107 polyunsaturated fatty acid, is high commercially valued and commonly sold as a fresh fillet in
108 markets (Volpe et al., 2015). However, the fresh fillet is prone to receive fat oxidation, protein
109 degradation, and decomposition of bacteria and endogenous enzymes, resulting in the spoilage and
110 decline of its commercial values (Zhao et al., 2021). Thus, the application of biodegradable film
111 in fillet packaging can inhibit lipid oxidation and protein deterioration during refrigerated storage.

112 To the best of our knowledge, introducing CIN-loaded CHNPs (CCNPs) into the design of
113 biopolymer-based nanocomposite films with tailored functionalities has not been investigated yet.
114 Hence, in this work, two hypotheses could be established: first, that CCNPs with adequate physico-
115 chemical attributes may be synthesized and second, that these NPs may enhance the functional
116 properties of nanocomposite films. The main objective of this study is to evaluate the influence of
117 CCNPs on the CIN release behavior, physico-mechanical, microstructural, and
118 antimicrobial/antioxidant properties of the films obtained. The effect of bionanocomposite films
119 was also studied on the preservation of rainbow trout fillet.

120 **2. Materials and methods**

121 *2.1. Materials*

122 Medium molecular weight chitosan (CH) (M_w 190-310 kDa, 75-85% degree of deacetylation),
123 poly(vinyl alcohol) (PVA) (M_W: 89000-98000, 99% hydrolyzed), gelatin from cold-water fish skin
124 (FG), sodium tripolyphosphate (TPP), 1,1-diphenyl-2-picrylhydrazyl (DPPH), 1-butanol,
125 thiobarbituric acid (TBA) reagent, and tween 80 were purchased from Sigma-Aldrich (St. Louis,
126 MO, USA). Cinnamaldehyde (CIN), trichloroacetic acid (TCA), glacial acetic acid, and glycerol
127 were obtained from Merck (Darmstadt, Germany). Potassium ferricyanide was supplied by
128 Rankem (Haryana, India). *Staphylococcus aureus* (PTCC 1337), *Listeria monocytogenes* (PTCC
129 1298), *Salmonella enteritidis* (PTCC 1709), and *Escherichia coli* (PTCC1330) were provided by
130 the Persian Type Culture Collection (Tehran, Iran). Subculturing was carried out monthly to
131 maintain bacterial livability. All strains were kept in tryptic soy broth (TSB) (Scharlab, S.L.,
132 Barcelona, Spain) supplemented with 30% glycerol at -20 °C until used.

133 *2.2. Preparation of CIN-loaded CHNPs (CCNPs)*

134 CCNPs were prepared *via* the ionotropic gelation method according to our previous study
135 (Hosseini, Zandi, Rezaei, & Farahmandghavi, 2013). In brief, 0.5 mg/mL of CH was prepared in
136 1% (v/v) aqueous acetic acid solution by stirring overnight at ambient temperature. After adjusting
137 the pH to 5 using 10 M NaOH, the prepared solution was then centrifuged for 30 min at 9000 rpm;
138 the supernatant was gathered and filtered by 1 μm pore size filters. Tween 80 (HLB 15.9, 0.225 g)
139 was then added to the solution as a surfactant and stirred at 25 °C for 30 min to acquire a
140 homogeneous mixture. CIN (0, 0.05, 0.125, and 0.25 g) was dissolved separately in CH_2Cl_2 (4
141 mL) and then this oil phase was gradually dropped into the aqueous CH solution (40 mL) under
142 magnetic stirring in an ice-bath condition to obtain an oil-in-water emulsion. Afterwards, the TPP
143 solution (0.4% (w/v), 40 mL) was added dropwise into the emulsion with moderate stirring for 40
144 min. The CCNPs were collected by centrifugation at 9000 × g for 30 min at 4 °C and were
145 subsequently washed several times with deionized water. The CCNPs were re-suspended in water,
146 sonicated, and freeze-dried for further use.

147 *2.3. Preparation of bionanocomposite films*

148 Bionanocomposite films were prepared using the casting method as described in our earlier work
149 (Hosseini, Rezaei, Zandi, & Farahmandghavi, 2015b) with slight modifications.
150 40CH/40PVA/20FG was selected for the inclusion of the CCNPs because this formulation
151 presented the best physico-mechanical properties in the previous study which aimed to develop
152 ternary films based on these polymeric materials (Ghaderi et al., 2019). In brief, the CH film-
153 forming solution (FFS) (1.5%, w/v) was obtained by dissolving 1.5 g of CH in 1% acetic acid,
154 stirred overnight at room temperature. The PVA solution (2%, w/v) was prepared by dissolving 2
155 g PVA in 100 mL of distilled water under magnetic stirring at 85 °C for 2 h. Subsequently, the CH
156 and PVA solutions were blended (in a proportion of 1:1, v/v) to form a homogeneous CH/PVA

157 blend solution. The FG solution (2%, w/v) was also prepared by dissolving 2 g of gelatin in 100
158 mL of distilled water for 30 min and then heated at 45 °C for 45 min under continuous stirring. To
159 prepare optimum ternary blend films, the FG solution was added to the CH/PVA FFS blend at a
160 mass ratio of 20%. The resulting mixture was warmed and stirred for 30 min at 45 °C to obtain a
161 good blend. Glycerol (0.3 g/g dry matter) was added as a plasticizer and solutions were heated
162 again for 30 min at 45 °C. CHNPs containing different quantities of CIN (0, 0.05, 0.125, and 0.25
163 g) at a loading concentration of 6% (w/w) were first dispersed into distilled water and then
164 sonicated for 10 min. Then, the CCNP suspensions were added dropwise to the FFSs and gently
165 stirred for 60 min. After vacuum degassing to remove air bubbles, 15 mL of the dispersions were
166 poured into polystyrene Petri dishes (8 cm in diameter) and dried in an oven at 40 °C for 48 h. The
167 dried films were conditioned at 25 °C with 50 ± 4% relative humidity for 48 h until further analysis.
168 The corresponding films prepared by the above solutions were named CPF-CCNPs0, CPF-
169 CCNPs0.05, CPF-CCNPs0.125, and CPF-CCNPs0.25.

170 *2.4. Characterization of CCNPs and bionanocomposite films*

171 *2.4.1. Characterization of CCNPs*

172 The diameter and size distribution of the nanoparticle suspension was measured with the Zetasizer
173 Nano ZS instrument (Malvern Instruments Ltd.) on the basis of the dynamic light scattering (DLS)
174 technique. A morphological analysis was carried out by VEGA II scanning electron microscopy
175 (SEM, TESCAN, Czech Republic) and CM30 high-resolution transmission electron microscopy
176 (HRTEM, Philips, USA). For SEM, a drop of diluted nanoparticle suspensions (0.05 mg/ml) was
177 placed on a glass substrate, air-dried, and coated with gold so as to obtain a conducting surface,
178 and then analyzed. For HRTEM, a drop of the diluted sample solution was placed on a carbon-

179 coated grid, and surplus liquid was wicked away. The grid was then stained using 2% uranyl
180 acetate for 4 min and air-dried after the surplus stain was wicked away. After 4 min, the grid was
181 analyzed with HRTEM at a voltage of 200 kV.

182 *2.4.2. Characterization of the films*

183 *2.4.2.1. Film thickness*

184 Film thickness was determined using a digital micrometer (Mitutoyo Manufacturing Co. Ltd.,
185 Tokyo, Japan) with an accuracy of 0.001 mm at 9 random points around the film, and average
186 values were used in calculations.

187 *2.4.2.2. Mechanical behavior*

188 The tensile properties (tensile strength (TS) and elongation at break (EAB)) of the CPF-CCNPs
189 bionanocomposite films were examined by using a TVT-300Xp Universal Testing Machine
190 (Perten, Sweden) according to ASTM standard method D 882-09 (ASTM, 2009) with slight
191 modifications. Rectangular film specimens were prepared (10 mm × 60 mm) and conditioned at
192 23 ± 2 °C and 53 ± 2% RH for 48 h. The initial grip separation and cross-head speed were set at
193 30 mm and 1 mm/min, respectively. All measurements were tested at least 5 times simultaneously.

194 *2.4.2.3. Water vapor permeability (WVP)*

195 The water barrier characteristics of the films were determined in triplicate following a standard
196 method (ASTM E96-05) (ASTM, 2005). The samples were mounted on top of glass test cups
197 containing 6 mL of distilled water and sealed tightly. Then, the cells were placed in a desiccator

containing silica gel (0% RH; at 20 °C), and the cup was weighed every 2 h for up to 12 h. The WVP was calculated by Eq. (1):

(1)

where WVTR is the water vapor transmission rate (g mm/kPa h m^2) computed from the slope of the straight line divided by the exposed film area (m^2), L is average film thickness (mm), and ΔP is the difference in partial pressure (kPa).

2.4.2.4. Water contact angle

The surface hydrophilic/hydrophobic attributes of the bionanocomposite films were tested using a PG-X goniometer (PG-X, Switzerland) by a sessile drop method. A drop of deionized water (5 µl) was deposited on the film, photographed immediately and data was recorded after 0 and 10 s. Five measurements were conducted for each sample.

2.4.2.5. Surface color measurements

A colorimeter apparatus (BYK Gardner, USA) was used to determine the color of the films. Formerly, the instrument was calibrated using a standard white plate (L= 94.61, α = -0.89 and b= 0.57). The calculated parameters were L^* (lightness), a^* (redness/greenness), and b^* (yellowness/blueness) values. Total color variation from the standard (ΔE) was calculated based on Eq. (2):

(2)

2.4.2.6. Light transmission and opacity

217 The barrier properties of the CPF-CCNPs bionanocomposite films against UV and visible light
218 were measured at the ultraviolet and visible range (200-800 nm) onto rectangular film samples (1
219 × 4 cm) using a UV-vis spectrophotometer (UV-2600, Shimadzu, Kyoto, Japan) following the
220 previously described method (Fang, Tung, Britt, Yada, & Dalgleish, 2002). Film opacity was also
221 calculated using Eq. 3:

222 (3)

223 Where Abs 600 is the value of absorbance at 600 nm and x is the film thickness (mm).

224 *2.4.2.7. FT-IR vibrational spectroscopy*

225 Fourier transform infrared spectroscopy measurements were obtained using an FT-IR spectrometer
226 (Perkin Elmer, Spectrum Version 10.03.06, Waltham, MA, USA) equipped with an attenuated
227 total reflection (ATR) accessory. Spectra were recorded under the scan range of 4000-400 cm^{-1} at
228 a scan rate of 32 scans and spectral resolution of 4 cm^{-1}.

229 *2.4.2.8. X-ray diffraction (XRD)*

230 The XRD patterns of the bionanocomposite films were collected from a Siemens D5000 X-ray
231 diffractometer with Cu-Kα radiation at a wavelength of 1.78901 Å. The intensity in the spectra
232 was measured as a function of 2θ in the range of 5-80 at an increment of 0.04°/min.

233 *2.4.2.9. Differential scanning calorimetry (DSC)*

234 The calorimetric analysis was performed on a DSC-200 F3 (NETZSCH, Germany) under an
235 atmosphere of nitrogen at a flow rate of 100 mL/min. The film samples (approximately 7.0 mg)

236 were tightly encapsulated in aluminum pans and then scanned in the range of 25 to 400 °C at the
237 heating rate of 10 °C/min.

238 *2.4.2.10. Thermogravimetric analysis (TGA)*

239 TGA analysis of the CPF-CCNPs films was performed at a heating rate of 10 °C/min from 25 °C
240 to 600 °C by a thermal gravimetric analyzer (Perkin-Elmer PYRIS I, USA). All samples were
241 placed in a dry environment prior to testing and about 8.0 mg of the films were used for testing.
242 The results were recorded as TG and DTG-scanned curves.

243 *2.4.2.11. SEM observation*

244 The surface and cross-section microstructures of the films were obtained using a scanning electron
245 microscope (XL30 ESEM, Philips, Netherlands) with an accelerating voltage of 20 kV. Cross-
246 sectional views of the samples were prepared by freeze-fracturing in a liquid nitrogen bath. Finally,
247 samples were mounted on an aluminum stub and sputter-coated with a thin layer of gold before
248 imaging.

249 *2.4.2.12. Atomic force microscopy (AFM) imaging*

250 The surface morphology and roughness of the film samples were analyzed by an atomic force
251 microscope (CP-R, Veeco Instruments, USA) operated in contact mode by a triangular cantilever
252 with a spring constant of 50 N/m. Two quantitative parameters of roughness were calculated using
253 ProScan software (version 1.7): average roughness (*R*a), and the root-mean-square roughness (*R*q).

254 *2.4.2.13. CIN release experiment*

255 CIN release studies were performed by immersing the film (2 cm × 2 cm) into 50 mL of PBS
256 (pH=7.4) under stirring (100 rpm) at 37 °C according to the method reported by Wu et al. (2019)
257 with some modifications. At designated time intervals, 3 mL of the release media was taken out
258 and an equal volume of fresh buffer was replaced. The released CIN was analyzed using a UV-vis
259 spectroscopy (λ=285 nm), and its concentration was calculated using the standard curve
260 established using the PBS medium. The total mass of released CIN M_i at time i was calculated
261 from the following equation:

262 (4)

263 where C_i is the concentration of released CIN in the solution at the time i, V is the total volume of
264 release solution, and V_s is the sample volume.

265 *2.4.2.14. Antimicrobial properties*

266 The disk-diffusion assay was used to assess the antibacterial activity of the CCNPs functionalized
267 CPF ternary films against four common Gram-positive (*S. aureus* and *L. monocytogenes*) and
268 Gram-negative bacteria (*S. enteritidis* and *E. coli*) following our previously described method
269 (Javidi, Hosseini, & Rezaei, 2016). The films were cut into 10 mm diameter disks and placed on
270 the surface of sterile agar plates previously seeded with 0.1 mL of inoculum containing 10^6
271 CFU/mL of tested bacteria. After that, the plates were incubated at 37 °C for 24 h and the diameter
272 of the inhibition zones (mm) was measured. All determinations were performed in triplicate.

273 *2.4.2.15. Antioxidant activities*

274 *2.4.2.15.1. DPPH assay*

275 The free radical scavenging activity of the nanocomposite films was evaluated based on the
276 modified procedure of Lian, Peng, Shi, and Wang (2019). Briefly, film samples were cut and
277 dissolved in 10 mL of methanol and centrifuged at 150 rpm for 12 for 30 min at 25 °C to obtain
278 the film extract solution. Afterward, 200 µL of film extracts were mixed with 2 mL of 1 mM
279 methanolic solution of DPPH. The mixture was shaken vigorously and left for 30 min in the dark;
280 the absorbance was read spectrophotometrically at 517 nm and the DPPH radical scavenging
281 activity was calculated by Eq. 4:

282 DPPH scavenging activity (%) - (5)

283 where A_{blank} and A_{sample} are the absorbance values of the DPPH solution without and with the
284 presence of the sample solutions. Each sample was measured in triplicate.

285 *2.4.2.15.2. Ferric reducing antioxidant power (FRAP) assay*

286 FRAP of the CPF-CCNPs nanocomposite films was carried out as described by Yıldırım, Mavi,
287 and Kara (2001) with slight modifications. Briefly, 500 µL of 0.1 M phosphate buffer and the same
288 volume of potassium ferricyanide (1%, w/v) were mixed with 200 µL of the film extract solution
289 and reacted at 50 °C for 20 min. Then, 500 µL of TCA (10%, w/v) were added and the mixture
290 was centrifuged for 10 min at 4000×g. Finally, 500 µL of the supernatant solution of each sample
291 mixture were mixed with 500 µL of distilled water and 100 µL of ferric chloride (0.1%, w/v). After
292 30 min of incubation at room temperature, the absorbance of the resulting solutions was read at
293 700 nm.

294 *2.5. Fish storage trial*

295 *2.5.1. Sample preparation*

296 Freshwater rainbow trout (*Oncorhynchus mykiss*) with an average weight of 250-300 g were
297 acquired at a specialized local market. Proximate analysis of the raw muscle was carried out
298 showing the following results: 69.17 ± 1.94% moisture, 21.85 ± 1.34% total protein, 1.97 ± 0.1%
299 ash, and 6.82 ± 1.59% total fat. Fish was cleaned, gutted, headed, and then filleted by hand. The
300 fillets were randomly divided into 3 batches: control fillets without wrapping (Control) and fillets
301 wrapped with the different sample films: CPF, wrapped with CPF film, CPF-CCNPs0.25: wrapped
302 with CPF-CCNPs0.25 nanocomposite film. The freshness of the fillet was determined at 0, 4, 8,
303 12, and 16 days during storage.

304 *2.5.2. pH assay*

305 pH measurement was performed as described by Zhao et al. (2021). 5 g of the samples with 45 mL
306 of distilled water were homogenized thoroughly for 1 min, followed by standing for 30 min. The
307 pH value of the homogenate was measured using a digital Jenway 3510 pH-meter (Jenway,
308 Staffordshire, UK).

309 *2.5.3. Thiobarbituric acid values (TBARS)*

310 TBARS values were measured according to the method described by Zhao et al. (2021) with some
311 modifications. In brief, 10 g of the fillet sample was homogenized with 25 mL of 7.5% (w/v)
312 trichloroacetic acid, then centrifuged at 5000 rpm for 10 min and filtered through Whatman no. 1
313 paper. The mixture of the filtrate and 0.02 M TBA reagent (1:1, v/v) was incubated at 90 °C for
314 15 min. After cooling under tap water, the absorbance of the mixture was measured at 532 nm

315 using a Biochrom WPA Biowave II UV-vis spectroscopy (Cambridge, UK), and the TBARS
316 readings were expressed as mg MDA/kg.

317 *2.5.4. Color parameters*

318 The surface color of rainbow trout fillets during chilled storage at 4 °C was recorded using a
319 colorimeter apparatus (BYK Gardner, USA), and the results were expressed as CIE L* (lightness),
320 a* (redness/greenness), and b* (yellowness/blueness) tristimulus coordinates of the color space.

321 *2.5.5. Microbiological assays*

322 Ten grams of fish sample were added to 90 mL of 0.85% (w/v) sterile saline solution. The mixture
323 was homogenized using a Stomacher blender (Model HBM-400B; HBM Biomed, Tianjin, China)
324 for 2 min, followed by serially diluted ten-fold using sterile saline solution. A 0.1 mL of
325 appropriate dilution was smeared onto the plate count agar plates (PCA, Merck) and incubated at
326 37 °C for 24 h for total viable counts (TVC) and 10°C for 7 days for psychrotrophilic counts (PTC)
327 (Sallam, 2007).

328 *2.6. Statistical analysis*

329 To investigate the difference among different variables, an ANOVA (one-way analysis of
330 variance) followed by the least significant difference (LSD) test were performed ($p \leq 0.05$). Data
331 were drawn by Origin Pro 2018.

332 **3. Results and discussion**

333 *3.1. Characterization of CCNPs*

334 The morphologies of the CCNPs were visualized using SEM and TEM (Fig. 1A and B). The SEM
335 image in Fig. 1A shows that the positively charged amino groups ($-NH_3^+$) in CH could be ionically
336 crosslinked with the negatively charged tripolyphosphate groups ($-P_3O_{10}^{5-}$) of TPP to form regular
337 spherical NPs with a uniform particle size. However, some NP aggregation was observed, which
338 can be attributed to the interaction of surface tension and electrostatic force between particles (Kuai
339 et al., 2020); this also may be due to hydrogen bonding interactions between NPs in the freeze-
340 drying process (Fan, Yan, Xu, & Ni, 2012). TEM imaging was extensively used to investigate the
341 NPs morphology, as well as their size. TEM micrograph also indicated the spherical shape and
342 smooth surface of the prepared CCNPs (Fig. 1B), showing a predictably smaller diameter than that
343 obtained from DLS measurements; this may be due to the shrinkage of the NPs during the drying
344 process (TEM sample preparation) (Hosseini, Soofi, & Rezaei, 2021). A similar morphology was
345 observed by Wu et al. (2019) for gallic acid-loaded CHNPs. DLS was also employed to investigate
346 the average hydrodynamic diameter, PDI, and ζ-potential of the CCNPs. In Fig. 1C, the size
347 distribution profile of the CCNPs had an average diameter of 370.3 nm in narrow size distribution
348 (PDI=0.166). ζ-potential is utilized as an index to evaluate the stability of the colloidal dispersion
349 since it is a measure of the particle surface charges. In Fig. 1D, the ζ-potential of the CCNPs
350 prepared in the present study was found to be +32.2 mV (larger than ± 30 mV), which suggested
351 that the NPs could be stabilized by electrostatic repulsion interactions (Mo et al., 2021).

352 *3.2. Characterization of bionanocomposite films*

353 *3.2.1. Film thickness*

354 The thickness of the film is an important parameter that directly affects the physico-mechanical
355 attributes, such as barrier and tensile properties. The incorporation of the CCNPs significantly

356 increased ($p < 0.05$) the thickness of the CPF ternary films (varied from 0.046-0.050 mm) (Table
357 1), which may be due to the increase in the amount of solid content in FFSs (Sun et al., 2020). A
358 similar trend was observed for nanocomposite films composed of pullulan and lysozyme
359 nanofibers (LNFs) (Silva, Vilela, Almeida, Marrucho, & Freire, 2018). On the other hand, Wu et
360 al. (2020) found that the thicknesses of konjac glucomannan-based films were not significantly
361 altered by the incorporation of oxidized chitin nanocrystals (O-ChNCs) or red cabbage
362 anthocyanins (RCA). These changes could be due to the nature of the polymer, nanoparticles, and
363 plant-derived phenolic compounds used in different studies.

364 *3.2.2. Mechanical properties*

365 TS (tensile strength) and EAB (flexibility) are key parameters needed for food packaging films to
366 keep their integrity and tolerate external stress during their transport and exposition lifecycle. Fig.
367 2A displays the representative stress-strain (σ-ε) curves of the different film samples, while the
368 corresponding tensile properties are listed in Table 1. From Fig. 2A, a linear drawing process in
369 the stress-strain in the control CPF and bionanocomposite films was visible. With the addition of
370 the CCNPs in the CPF matrices, the TS of the resulting nanocomposites increased, while the EAB
371 values decreased; this reinforcement may be attributed to the uniform distribution and interface
372 compatibility of the CCNPs within the CPF ternary matrices, as evidenced by SEM results (see
373 section 3.2.10). As presented in Table 1, filling the polymer with the CCNPs (at various bioactive
374 loading, 0-0.125 g) significantly improved ($p < 0.05$) the TS of the films compared with that of the
375 control CPF film, thus corroborating that NPs enhance the functional properties of nanocomposite
376 films. This indicated that the CCNPs were able to restrict chain mobility at the molecular level as
377 well as to allow stress transfer from the polymer chains to the CCNPs when tensile force is applied
378 (Trinh, Chang, & Mekonnen, 2021). This phenomenon could be related to the homogeneous

379 dispersion of NPs in the film matrix, thereby forming a new hydrogen bond between the filler and
380 the polymer matrix (Wu et al., 2019). Many studies have also found larger TS values in
381 nanocomposite films than in neat films (Al-Tayyar, Youssef, Al-Hindi, 2020b; Wu, Sun et al.,
382 2019). However, at the highest CIN loading (*i.e.,* for CPF-CCNPs0.25), the TS of the film
383 decreased, although it was still higher than that of the neat CPF film. This was possibly due to the
384 NP aggregation that arises from the interaction of surface tension and electrostatic force between
385 particles in the bionanocomposite matrix, which are exacerbated by the drying step and ultimately
386 result in a TS reduction (Kuai et al., 2020). This result is in agreement with the data obtained from
387 SEM (Fig. 5C), where an enhancement of the agglomeration rate of CHNPs is observed at higher
388 amounts of CIN loading (CPF-CCNPs0.25). The TS values of these bionanocomposite films were
389 higher than those of chitosan/poly(vinyl alcohol)/zinc oxide nanoparticles bionanocomposites (18-
390 37.5 MPa) prepared by the solvent casting method (Al-Tayyar et al., 2020b), and were comparable
391 to those of typical packaging plastics, *e.g.,* low-density polyethylene (LDPE) (15.2-78.6 MPa),
392 high-density polyethylene (HDPE) (17.9-33.1 MPa), isotactic polypropylene (iPP) (29.3-38.6
393 MPa) but slightly lower than those of polystyrene (PS) (45-83 MPa) (Castilho, Mitchell, & Freire,
394 2009) revealing its high potential as packaging material.
395 On the contrary, EAB values decrease with the incorporation of the CCNPs into the polymer matrix
396 from 128.39 ± 11.32% (control CPF film) to 90.82 ± 5.25% (CPF-CCNPs0.25), which could be
397 attributed to an improvement on the rigidity of the bionanocomposite films. Furthermore, CCNPs
398 can disperse and entangle with the polymer matrix, filling void spaces and consequently decreasing
399 elasticity (Cui et al., 2020).

400 *3.2.3. Water vapor permeability (WVP)*

401 WVP represents the barrier property of the material against water vapor, and a low WVP is
402 generally required for food packaging. WVP is also very significant for fresh foodstuffs,
403 considering that dehydration and moisture absorption must be avoided (Al-Tayyar et al., 2020a).
404 The effects of the CCNPs on the WVP values of the ternary CPF films are shown in Table 1. The
405 WVP value of the control CPF film was 0.785 ± 0.053 g mm/kPa h m^2, which is several times
406 lower than that reported, for instance, for agar/alginate/collagen ternary film, i.e., 5.44 g mm/kPa
407 h m^2 (Wang & Rhim, 2015). As evidenced in Table 1, no significant differences are observed in
408 the WVP of films after CCNP addition ($p > 0.05$). It seems that the hydrophilic nature of CHNPs
409 allows for the easy absorption of water molecules, resulting in no significant change in WVP
410 values in these films (Vahedikia et al., 2019). However, the slight increase in the WVP of the films
411 reinforced with CHNPs loaded with higher amounts of CIN (*i.e.,* for CPF-CCNPs0.125 and CPF-
412 CCNPs0.25) as compared with other films, is probably due to nanofiller aggregation during solvent
413 evaporation (Norcino et al., 2020). In any case, when compared with synthetic polymeric films,
414 WVP values are similar to those observed in cellophane films (0.248 g mm/kPa h m^2) but higher
415 than those observed in low-density polyethylene (LDPE) films (0.0072 g mm/kPa h m^2).

416 *3.2.4. Surface wettability measurements*

417 Ideal biopackaging materials should have sufficient hydrophobicity to maintain their structural
418 integrity in a wet environment. The surface wettability and hydrophilicity of the bionanocomposite
419 films were examined by measuring the contact angle (CA) of the water droplet deposited onto the
420 film's surface and the results are shown in Table 1. The CA value of the control CPF film was
421 73.85°, higher than the value reported in the literature in a CH/PVA film (69°) (Narasagoudr,
422 Hegde, Vanjeri, Chougale, & Masti, 2020). As it is described in Table 1, the incorporation of the
423 CCNPs did not contribute much to alter the wettability of the resulting nanocomposite films, which

424 might be due to the hydrophilic nature of the NPs (Vahedikia et al., 2019). The surface wettability
425 of nanocomposite films is not only related to the interactions between the biopolymer and the NPs,
426 but also to the hydrophobicity/hydrophilicity of the nanomaterial itself (Mo et al., 2021). However,
427 it is important to note that all developed films had hydrophobic surfaces as they exhibited contact
428 angles $\theta > 65°$ (Hambleton, Fabra, Debeaufort, Dury-Brun, & Voilley, 2009).

429 *3.2.5. Optical parameters*

430 Both color and transparency of packaging films play an important role in their appearance and
431 consumer satisfaction. All the films exhibited transparency, surface smoothness, and
432 homogeneous appearance, as observed in the photographs (Fig. 1 of Supplementary material).
433 However, the films containing the CCNPs were slightly opaque compared with films without the
434 NPs. The effects of the NPs on the color parameters L^* (lightness), a^*(redness/greenness), b^*
435 (yellowness/blueness), and ΔE^* (total color difference), and the opacity of the films are listed in
436 Table 2. The apparent color of the film samples as determined by Hunter color values, indicates
437 that the ΔE of the pristine CPF film increased slightly after CCNP incorporation (Table 2), which
438 is mainly due to an increase in Hunter *a*- and *b*-values and a decrease in *L*-values. In particular, *b*-
439 values showed a greater difference ($p < 0.05$), indicating that the film gradually changed from
440 colorless to yellow. Similar color changes were observed for gelatin films incorporated with
441 natamycin-loaded zein/casein nanoparticles (Mo et al., 2021).

442 In terms of opacity, the obtained value in the CPF ternary film was 1.37 ± 0.09 AU/mm (Table 2),
443 which is closer to values obtained in OPP (oriented polypropylene) (1.67), a commercial film used
444 for packaging purposes (Guerrero, Stefani, Ruseckaite, & de la Caba, 2011). As summarized in
445 Table 2, CCNP incorporation triggered the opacity of the ternary films, reaching a value of 3.68 ±
446 0.11 AU/mm at maximum CIN-loaded NPs concentrations (*i.e.,* CPF-CCNPs0.25). The drop in

447 transparency of films containing the NPs was ascribed to the ability of the particles to prevent the
448 transmission of light through the films (Pérez-Córdoba et al., 2018). This effect is also probably
449 due to the increased thickness of films with NPs, which could enhance the reflection and absorption
450 of light (Xue, Gu, Wang, Li, & Adhikari, 2019).

451 *3.2.6. Light transmittance of bionanocomposite films*

452 Since one of the common oxidation initiators in food systems is UV light (in the range of 200-280
453 nm), paying attention to lipid oxidation due to UV light is important. The transmission of UV and
454 visible light at a selected wavelength (200-800 nm) in the films is shown in Fig. 2B. The
455 transmission of UV light was very low at 200 nm in all films (0.07-0.1%), and at 280 nm, in the
456 bionanocomposite films, the transmission decreased from 24.60 (for the neat CPF film) to the
457 range of 2.07-4.83% when the films reinforced with CHNPs were loaded with different amounts
458 of CIN (from 0-0.25g); this may be attributed to the scattered and/or reflected light at the interface
459 of the loaded CCNPs in the films, thus reducing the amount of light passing through the films (Wu
460 et al., 2020). It is also noteworthy that the rate of light transmittance at 280 nm was markedly lower
461 when compared with that displayed by some conventional polymer films, *i.e.,* 71.78 and 27.64%,
462 for OPP and LDPE, respectively (Guerrero et al., 2011), demonstrating that prepared CPF-CCNPs
463 bionanocomposite films could protect foods from UV light-induced lipid oxidation, nutrient loss,
464 discoloration, and off-flavors.

465 In the visible range (350-800 nm), all bionanocomposite films showed a lower light transmission
466 than the control CPF film. As a result of the increased light-blocking properties (as discussed
467 above), films reinforced with the CCNPs also had lower transparency values than pure films. It
468 can be concluded that the CCNPs with light-scattering ability most likely contributed to the limited

469 light transmittance of the bionanocomposite films at both UV and visible light ranges, and are
470 more suitable for food packaging applications.

471 *3.2.7. ATR/FT-IR spectroscopy*

472 ATR-FTIR spectroscopy was performed to evaluate the interactions between the functional groups
473 of the polymer matrix and the CCNPs. The spectra of films from pure compounds (*i.e.,* CH, PVA,
474 and FG) are comprehensively discussed in our previous paper (Ghaderi et al., 2019), and the
475 spectra of films from selected formulations are shown in Fig. 3A. In the FT-IR spectrum of the
476 control CPF film (Fig. 3A-a), the peak at 3340 cm^{-1} corresponds to the stretching vibration of O-
477 H groups, and the peak at 2939 cm^{-1} corresponds to the asymmetric stretching mode of C-H (Mo
478 et al., 2021). The absorption band at 1735 cm^{-1} was assigned to the stretching vibrations of C=O
479 groups of the residual vinyl acetate units in the PVA backbone (Wu et al., 2018). The peaks at
480 approximately 1655, 1554, and 1248 cm^{-1} correspond to C=O stretching modes (amide I), N-H
481 deformation modes (amide II), and C-N and N-H stretching (amide III), respectively (Cazón,
482 Vázquez, & Velazquez, 2018).

483 The spectra of the bionanocomposite films showed distinctive peaks as compared with the control
484 film; however, some of the peaks shifted or disappeared with the incorporation of the CCNPs (Fig.
485 3A-b and c). It is observed that the peaks at 3340, 1655, and 1554 cm^{-1} are shifted to a lower
486 wavelength with the incorporation of the CCNPs, indicating the decreased stretching of free O-H
487 and/or N-H due to the hydrogen bonds formed between the NPs and the polymer molecules which
488 enhanced the tensile and water barrier properties of the nanocomposites (Wu et al., 2019).
489 Meanwhile, the bands at 1248 (amide III peak) and 1331 cm^{-1} (CH_3 symmetric deformation)
490 shifted to higher wavenumbers, suggesting the formation of additional hydrogen bonds between
491 CPF and the CCNPs in the bionanocomposite films (Wu et al., 2019). Also, the absorption peak at

492 about 1076 cm^{-1} corresponding to the C-O group (Pereira Jr, de Arruda, & Stefani, 2015) shifted
493 to a higher wavenumber (1092/1093 cm^{-1}) in films containing the CCNPs. However, the peaks at
494 2287 and 2045 cm^{-1} disappeared in the spectrum of the bionanocomposite films, indicating the
495 appearance of intermolecular hydrogen bonds (Wu et al., 2019).

496 *3.2.8. X-ray diffraction*

497 XRD analysis was used to examine a possible change of crystallinity in the obtained
498 bionanocomposite films. The XRD patterns of the pure CH, PVA, and FG films have been reported
499 in our recently published work (Ghaderi et al., 2019). As shown in Fig. 3B-a, the XRD pattern of
500 the control CPF film displays two main diffraction peaks at $2\theta = 10.65°$, corresponding either to
501 the crystalline triple helix structure of FG or to the relatively regular crystal lattice of CH, and 2θ
502 $= 22.48°$, characteristic of an amorphous phase (Pérez-Córdoba et al., 2018). The incorporation of
503 the CCNPs decreased the crystallinity of the control CPF film. When the CCNPs (either in the
504 blank (CCNPs0) or loaded with CIN (CCNPs0.25)) were added to the polymer matrices, the peak
505 at $2\theta = 10.65°$ disappeared (Fig. 3B-b and c), indicating that the addition of the NPs inhibited the
506 formation of triple helices. The triple helix structure in gelatin gels was mainly formed by
507 intramolecular hydrogen bonds and hydrogen bond hydration; the amino groups on the NPs could
508 form hydrogen bonds with gelatin chains and thus interfere with the triple helix structure (Kuai et
509 al., 2020). Also, the addition of the NPs changed the position and intensity of the second diffraction
510 peak of the control CPF film, demonstrating that CCNPs are able to change the intermolecular
511 structure of the film (Norcino et al., 2020).

512 *3.2.9. Thermal properties of bionanocomposite films*

513 *3.2.9.1. Differential scanning calorimetry (DSC)*

514 Thermal properties of the neat CPF and CPF-CCNPs nanocomposite films were analyzed by DSC
515 and TGA. The DSC curves of the pure ingredients (*i.e.,* CH, PVA, and FG) are also discussed in
516 our previous report (Ghaderi et al., 2019). Two major endothermic peaks at 147.8-169.1 °C and
517 282.8-285.4 °C can be clearly observed in all films (Fig. 3C). The first peak may be assigned to
518 the overlapping of different phenomena, such as the volatilization of adsorbed water, residual
519 acetic acid, the degradation of glycerol as a plasticizer, the helix-coil transition of gelatin, as well
520 as the melting temperature (T_m) of polymers (Nilsuwan, Benjakul, & Prodpran, 2018). The latter
521 peak also represented the thermal decomposition (T_d) due to the dehydroxylation of the PVA, the
522 pyrolytic decomposition of the CH backbone, the thermal decomposition of peptide bonds in the
523 main chain of gelatin, and the chemical degradation of CCNPs (Martucci & Ruseckaite, 2015).
524 Generally, the incorporation of the CCNPs increased the thermal stability of the polymer films,
525 thus exhibiting an improvement of the functional properties, as presented in the second hypothesis.
526 Compared with pure film (Fig. 3C-a), the endothermic peaks of the bionanocomposite films were
527 shifted towards higher temperatures (Fig. 3C-b and c), meaning that the intermolecular interactions
528 formed between the NPs and polymer molecules enhance the thermal stability of the
529 nanocomposite films (Cui et al., 2020). Concerning the melting enthalpy (ΔH_m), this was markedly
530 increased from 160.9 J/g (control film) to 311.1 J/g when the films were reinforced with the highest
531 amount of CIN-loaded NPs (CPF-CCNPs0.25). The higher enthalpy values for the nanocomposite
532 films indicated that they presented a higher level of renaturation compared to the neat film, leading
533 to an improved strength value (Pérez-Córdoba et al., 2018), as demonstrated by TS data (Table 1).

534 *3.2.9.2. Thermogravimetric analysis (TGA)*

535 The thermal gravimetric analyzer was also used to evaluate the thermal stability of CPF-CCNPs
536 nanocomposite films, and the results were recorded as TG and DTG scanned curves, which

537 reflected the residual mass ratio and the mass loss of the films with increasing temperature,
538 respectively. As shown in Fig. 4A, the residual mass of CPF-based films with CCNPs (either blank
539 (CCNPs0) or loaded with CIN (CCNPs0.25)) was obviously higher than that of CPF-based films
540 without CCNPs, therefore, the incorporation of the CCNPs significantly enhanced the thermal
541 stability of the CPF films. The mass of CPF-CCNPs0 and CPF-CCNPs0.25 remained 23.42% and
542 29.65%, respectively, when the temperature rose to around 600 °C. By contrast, the weight of CPF
543 only remained 16.31%. According to the DTG curves of the CPF-CCNPs films (Fig. 4B), all
544 samples had three mass loss stages in the same temperature range during the thermal
545 decomposition process. The first stage, between 25-230 °C, mainly corresponded to the
546 evaporation of physically weak and chemically strong bound water as well as the volatilization of
547 glycerol (Yuan et al., 2021). In the second stage, between 230-350 °C, a large loss of weight
548 occurred (~33.8-37.5%), which may be related to the polysaccharide pyrolytic decomposition of
549 the CH, the dehydroxylation of the PVA, the chemical degradation of FG, CHNPs and CIN
550 (Hosseini et al., 2016; Sun et al., 2020). In the final stage, between 350-600 °C, the reduced weight
551 loss could be ascribed to the thermal decomposition of char (Sun et al., 2020).

552 *3.2.10. Film microstructure*

553 To further characterize bionanocomposite films for their morphological changes related to the
554 influence of the CCNPs, the surface and cross-section topography of the films were analyzed by
555 SEM. The pure CPF film possesses a homogeneous and smooth surface without any pores and/or
556 cracks and with excellent structural integrity (Fig. 5A), indicating the good compatibility of the
557 three polymers (*i.e.,* CH, PVA, and FG). The surface of the bionanocomposite film is relatively
558 compact and smooth with homogeneous granules after adding blank NPs (CPF-CCNPs0) (Fig.
559 5B), confirming the excellent phase compatibility between particles and polymer matrices, which

560 may improve the physico-chemical properties of the resultant films (Wu et al., 2020). The uniform
561 distribution of the CCNPs also corroborated the good dispersion procedure used in this research.
562 As illustrated in Fig. 5C, when the NPs loaded with 0.25 g CIN were added to the polymer matrices
563 (CPF-CCNPs0.25), although some NPs appeared as light bumps in the nanocomposite films, no
564 significant particle aggregation was found on the fracture surface, revealing that the CCNPs were
565 still distributed in the polymer matrices at this loading level. A similar microstructure has been
566 also reported in konjac glucomannan (Wu et al., 2019), zein (Cui et al., 2020; Vahedikia et al.,
567 2019), and gelatin (Hosseini et al., 2015b; Wang et al., 2020) films reinforced with CHNPs.
568 In cross-section micrographs, the control CPF film had a smooth and compact structure (Fig. 5a),
569 as expected for a homogeneous material. As shown in Fig. 5b, a dense and rough microstructure
570 was found in the cross-section of the blank NP-doped ternary film (CPF-CCNPs0), which might
571 be due to the strong bonding between the NPs and the polymer chains (Wang et al., 2020).
572 Nevertheless, the films loaded with the highest amount of CIN-loaded NPs (CPF-CCNPs0.25) had
573 some discontinuous zones and became rougher than others (Fig. 5c); this might be associated with
574 the reduction in TS (Table 1). The increase in the surface coarseness of the nanocomposite films
575 has been previously reported (Kuai et al., 2020; Mirzaei-Mohkam, Garavand, Dehnad, Keramat,
576 & Nasirpour, 2020).

577 *3.2.11. Surface morphology analysis*

578 AFM was also conducted to characterize the surface morphology of the bionanocomposite films
579 obtained; furthermore, AFM allows for the plotting of a histogram in terms of the relative height
580 of every pixel recorded during the scan (Mohajer, Rezaei, & Hosseini, 2017). Typical 3D surface
581 topographic AFM images together with the corresponding height profiles are presented in Fig. 6.
582 The control CPF film showed a relatively smooth topography as indicated by the low R_a, R_q, and

583 peak height values (9.43, 12.65 nm, and 109 nm, respectively) (Fig. 6A), which is coincident with
584 the SEM results. By adding blank NPs (CCNPs0), the bionanocomposite film still showed a
585 smooth superficial topography with fine structures on a nanometric scale (Fig. 6B). The height
586 profile also showed that CPF-CCNPs0 had a minimum vertical distance of 85 nm, revealing the
587 establishment of some interactions between the NPs and polymer molecules by the formation of
588 intermolecular interactions, hydrogen bonding, etc. (Wang et al., 2020). However, the presence of
589 the CCNPs with the highest amount of CIN (CPF-CCNPs0.25) led to remarkable increases in the
590 roughness of the films, as indicated by higher R_a and R_q values (17.31 and 22.71 nm, respectively)
591 (Fig. 6C). This may be associated with the greater development of nanofiller aggregation during
592 the drying step, consequently producing irregularities on the film's surface. Likewise, Wu et al.
593 (2019) reported a significant increase in the surface roughness of a konjac glucomannan film after
594 gallic acid-loaded CHNPs were added.

595 *3.2.12. Release kinetics of CIN from*

596 To assay the release behavior and acquiring basic information for release kinetics, the
597 accumulative release percentages of CIN from CPF-CCNPs nanocomposites exposed to a
598 hydrophilic PBS medium were measured by monitoring the absorbance at λ_{max} = 285 nm during
599 72 h (Fig. 7). CIN is released from all the films in a two-step biphasic process; an initial burst
600 release (9.5-30.9%) within the first 12 h, which was mainly attributed to the release of
601 unencapsulated CIN, poorly entrapped and/or nanoparticle surface-adsorbed CIN
602 (Farahmandghavi, Imani, & Hajiesmaeelian, 2019; Kuai et al., 2020); and the subsequent slower
603 release, in which the accumulative release increased gradually before reaching a plateau (nearly
604 16.2-40.9% at 48 h) because longer time was required for the CIN molecules being enclosed into
605 the inner core of the CHNPs to be released through the longer pathway (Wang et al., 2017). In

606 fact, the CIN encapsulated in NPs need to diffuse to the surface of particles at a relatively slow
607 rate before diffusing from the surface of the particles to the CPF-CCNPs nanocomposite film,
608 eventually reaching the release equilibrium. In addition, the NPs formed intermolecular
609 interactions with the polymer molecules, which also led to the delayed release of CIN from the
610 film matrix (Mo et al., 2021). It is worth noting that a higher CIN content led to a higher cumulative
611 release, indicating that the release of the CIN from the bionanocomposite film matrix was primarily
612 controlled by the diffusion driving force generated by the change in incorporated CIN content (Wu
613 et al., 2020). However, most of the CIN present in CPF-CCNPs films was not released (remaining
614 59.1-83.8%) at the end of 72 h, which showed the durability of the biomolecule in the films. These
615 results indicated that CHNPs could effectively control the release by inhibiting the migration of
616 CIN. The low sustained and prolonged release of antimicrobial/antioxidant agents from
617 nanocomposites has a great potential for bioactive food packaging purposes.

618 *3.2.13. Antibacterial properties of the bionanocomposite films*

619 The antibacterial activities of pure CPF film and CPF-CCNPs bionanocomposite films were tested
620 against model Gram-positive (*S. aureus* and *L. monocytogenes*) and Gram-negative (*S. enteritidis*
621 and *E. coli*) bacteria and the results, evaluated by the disk diffusion assay, are presented in Table
622 3. The control film did not show any antibacterial activity against the studied microorganisms,
623 which could be associated with the limited diffusion of CH from the film to the adjacent agar
624 medium, as only the growth of organisms in direct contact with the active sites of CH is prevented
625 (Coma et al., 2002). It was also suggested that CH may only exhibit antimicrobial properties when
626 in a gelled or viscous acid solution form, where the polymer is soluble and carries a net positive
627 charge. According to Sahariah and Másson (2017), when the pH is lowered below 6.5, the amino
628 groups will protonate and get converted to the quaternary form ($-NH_3^+$), thereby giving a positive

629 charge to the polymer backbone and making it water soluble. The presence and the density of this
630 cationic charge is believed to be responsible for the efficient binding of CH to the anionic
631 components present in the bacterial cell wall/membrane (Raafat, von Bargen, Haas, & Sahl, 2008).
632 The films containing blank CCNPs (CPF-CCNPs0) and NPs loaded with 0.05 g CIN (CPF-
633 CCNPs0.05) showed no inhibitory action against the above-mentioned bacteria, similar to the
634 control ternary film. On the contrary, further CIN loading into NPs (CCNPs0.125 or CCNPs0.25)
635 enhances the antimicrobial activity of the nanocomposites, as evidenced by the diameter of
636 inhibition (Table 3). Fig. 2 of Supplementary material illustrates the representative pictures of the
637 inhibitory effect of the CPF films incorporated with the highest amount of CIN-loaded NPs (CPF-
638 CCNPs0.25) against the four tested microorganisms, as compared with the control. According to
639 the diameter of the zone of inhibition, CPF-CCNPs bionanocomposite films were more effective
640 against Gram-positive (*S. aureus* and *L. monocytogenes*) than Gram-negative (*S. enteritidis* and *E.*
641 *coli*) bacteria. It is hypothesized that this result may be attributable to the presence of the outer
642 membrane that surrounds the cell wall in Gram-negative bacteria, which limits the diffusion of
643 hydrophobic substances through its lipopolysaccharide covering (Burt, 2004). Overall, the low
644 antimicrobial activity of the bionanocomposite films can probably be due to the slow controlled
645 release of CIN from the CPF-CCNPs films, since in our study the active compounds were doubly
646 encapsulated, into the NPs and in the film matrix. Accordingly, the findings in our study are
647 consistent with those of other researchers that reported the effects of NPs in controlling diffusion
648 or enhancing the retention of antimicrobial agents by polymer matrices (Meira, Zehetmeyer,
649 Werner, & Brandelli, 2017; Wu, Zhu, et al., 2019). This suggests a controlled release behavior
650 which may be beneficial for films intended for long-term storage.

651 *3.2.14. Antioxidant activities of the bionanocomposite films*

652 *3.2.14.1. DPPH free radical scavenging activity*

653 Antioxidant packaging has received special attention since it can reduce the oxidation of food
654 products, which is the main reason of food spoilage after microbial growth (Vilela et al., 2018).
655 Free radical scavenging is thought to be one of the main mechanisms exhibited by antioxidants to
656 delay oxidative processes; DPPH is a stable free radical which accepts an electron or hydrogen
657 radical to become a stable diamagnetic molecule (Ksouda et al., 2019). The DPPH radical
658 scavenging activity of the CCNP-doped CPF films varied from 13.16 to 16.42%, whereas the pure
659 ternary films exerted a slightly lower effect (11.11% of inhibition) on the DPPH solutions (Table
660 3). The antioxidant activity of the film samples could be attributed firstly to amino ($-NH_3^+$) and
661 carboxyl (COOH) groups of CH or FG, and secondarily to hydroxyl (OH) and acetamino
662 (CH_3CONH-) groups of CH which can scavenge radicals (Kuai et al., 2020). Polyphenolic
663 compounds such as CIN have one or more aromatic rings with hydroxyl groups that can form
664 stable phenoxy radicals to quench free radicals (Ksouda et al., 2019). However, as
665 abovementioned, the films containing the CCNPs had a slightly higher DPPH scavenging activity
666 compared with the control ternary film. The reason for this slight difference may be attributed to
667 the slower release of encapsulated compounds in the film matrix (Kuai et al., 2020). The release
668 of CIN from the NPs requires two processes: the migration from the NPs to the film matrix,
669 followed by release from the film matrix; this reduced the amount of available CIN in the film.
670 Therefore, it is worth noting that the CIN in the NPs remained chemically stable and its antioxidant
671 activity could be effectively maintained after nanoencapsulation.

672 *3.2.14.2. Reducing power assay*

673 Since the antioxidant capacity of compounds involves different mechanisms of actions, it is of
674 great importance to combine more than one method to determine their *in vitro* antioxidant capacity.
675 Metal ions are known to catalyze lipid peroxidation, which can lead to the generation of both free
676 radicals and lipid peroxide radicals (Chentir et al., 2019). The reduction of ferric ion (Fe^{3+}) to the
677 blue ferrous form (Fe^{2+}) can be used as an indicator of electron-donating activity, which reflects
678 an important mechanism of antioxidant action (Ksouda et al., 2019). As depicted in Table 3, the
679 control CPF film imparted little reducing power activity ($OD_{700\ nm}$ = 0.08), and the addition of
680 CCNPs at different bioactive loadings (0-0.25 g) significantly ($p < 0.05$) improved this activity, as
681 suggested in the second hypothesis, reaching a maximum value of 0.16 ± 0.01 at the maximum
682 tested concentration (CPF-CCNPs0.25). Previous studies reported the capacity of antioxidant-
683 incorporated films, *e.g.,* fish protein hydrolysates ($OD_{700\ nm}$ = 0.3) (Kchaou, Jridi, Benbettaieb,
684 Debeaufort, & Nasri, 2020) and phycocyanin extract ($OD_{700\ nm}$ = 0.69) (Chentir et al., 2019) to
685 reduce ferric iron to ferrous iron.

686 *3.3. Application of the bionanocomposite film to fresh fillets preservation*

687 *3.3.1. pH value*

688 As can be seen in Fig. 8A, changes in pH value of different treatments showed the same trend in
689 which the values decreased initially and then increased. The initial pH decrease may be attributed
690 to the dissolution of CO_2 (arising from the glycogen degradation to lactic acid) in the fish sample,
691 while the increase of pH value is due to the production of alkaline compounds such as ammonia
692 and amines, due to proteins broken down by microorganisms (Zhao et al., 2021). The increase of
693 pH of fish fillets was significantly ($p < 0.05$) more rapid for control samples; specifically, pH
694 changed from 6.56 at day 0 to 7.31 at the end of the storage period. Taking into account that pH 7

695 is considered the limit value for acceptable quality (Zarandona et al., 2021), control samples
696 became non-acceptable before day 8 of storage. However, fish samples wrapped with CPF and
697 CPF-CCNPs0.25 films did not reach the pH limit value up to day 12 and this was extended until
698 the end of the storage for the samples wrapped with CPF-CCNPs0.25 nanocomposites.

699 *3.3.2. Thiobarbituric acid reactive substances (TBARS)*

700 TBARS analysis quantifies the presence of lipids' secondary oxidation substances, which major
701 component is malondialdehyde (MDA) (Shahidi, 1994). The TBARS value of fresh rainbow trout
702 fillets was 0.12 mg MDA/kg, and the values for all samples increased during storage (Fig. 8B).
703 Similarly, Jouki, Yazdi, Mortazavi, Koocheki, and Khazaei (2014) found TBARS of fresh rainbow
704 trout fillets to be below 0.2 mg MDA/kg. As shown in Fig. 8B, the TBARS values of the control,
705 CPF, and CPF-CCNPs0.25 treatments were increased from initial values to 0.34, 0.23, and 0.17
706 mg MDA/kg after 16 days storage, respectively. The lower TBARS values in the wrapped fillets
707 might have resulted from the well-known antioxidant property of amino or acetamino (CH_3CONH-
708) groups in CH (Kuai et al., 2020), which would form a stable fluorosphere with volatiles aldehydes
709 such as MDA. Furthermore, acidic amino acids (*e.g.,* aspartic and glutamic acids) existing in GE,
710 have powerful antioxidant capacities owing to the existence of excess electrons that can be donated
711 during interactions with free radicals (Hosseini, Soofi, et al., 2021). On the other hand, the
712 capability of bio-based films as a barrier to oxygen diffusion is another important aspect for
713 preventing lipid oxidation, in which, higher stability against oxidation was partly elucidated by a
714 lower matrix oxygen permeability (Vasile et al., 2016). According to Hosseini, Javidi, and Rezaei,
715 (2016), GE has sufficiently low oxygen permeability to serve as effective barrier biomaterials.
716 Phenolic components and aldehydes from CIN in CPF-CCNPs0.25 films could also act as electron
717 donors, metal chelators, and UV-visible light barriers to prevent lipid oxidation in fish samples

718 (Zhao et al., 2021). Zhao et al. (2021) revealed that edible films containing cinnamon-perilla
719 essential oil Pickering nanoemulsion postponed the production of TBARS during refrigerated
720 storage of red sea bream fillets.

721 *3.3.3. Color parameters*

722 Physicochemical changes during fish storage are known to cause changes in fish appearance
723 (Zarandona et al., 2021) and, thus, surface color was measured to analyze the effect of the
724 wrappings under study. As can be seen in Fig. 9A, after 16 days of storage, the L* value of the
725 control group was slightly lower than other groups because the CPF and/or CPF-CCNPs0.25 films
726 were wrapped on the surface of fillets, reducing exposure to air. Similarly, Zhao et al. (2021)
727 reported that the L* value of red sea bream fillets wrapped in a collagen-based film containing
728 cinnamon-perilla essential oil Pickering nanoemulsion was higher than that of control during
729 chilled storage, indicating a protective effect of chitosan against color changes. Concerning a*
730 (redness) parameter (Fig. 9B), the samples showed mean values in the range from 5.2 to 3.8,
731 similar to those found in the work of Yagiz, Kristinsson, Balaban, and Marshall (2007). Although,
732 the a* parameter decreased for all samples over time, nonetheless, the a* values for the trout
733 samples wrapped with CPF-CCNPs0.25 films were slightly higher compared to control and CPF
734 samples, which may be attributed to the phenolic components and aldehydes from CIN (Alves,
735 Rico, Vicente, Khmelinskii, & Vieira, 2018). Regarding the b* values, a significant ($p < 0.05$)
736 increase was observed in the whole storage period, independent of the different treatments used
737 (Fig. 9C). This yellowing effect may be related to the increase of volatile amines, as previously
738 shown in Atlantic horse mackerel fillets' with gallic acid-incorporated chitosan nanoparticles
739 (Zarandona et al., 2021).

740 *3.3.4. Microbiological analyses*

741 Fig. 10 shows the microorganism's evolution during storage. Initially, a load of total viable counts
742 (TVC) in the rainbow trout was 2.9 log CFU/g (Fig. 10A), which indicates good hygienic handling
743 of the raw material. The fish was considered fresh when the total bacterial count was 2-3 log
744 (CFU/g) in the fillets (ICMSF, 1986). Bacterial counts increased with an increase in storage time,
745 as the TVC of the control, CPF, and CPF-CCNPs0.25 treatments reached 7.75, 6.78, and 6.27 log
746 CFU/g, at Day 12, respectively. Considering the acceptable limit of 7 log CFU/g for fresh fish
747 (ICMSF, 1986), the shelf-life of the control group was 8 days while CPF and CPF-CCNPs0.25
748 films could extend the shelf-life of fillets to 12 days. These results are primarily due to the ability
749 of CPF-based films as a barrier to oxygen diffusion which inhibits the growth of aerobic bacteria
750 (Jouki et al., 2014). Likewise, differences ($p < 0.05$) in 0.3-0.5 log cycle counts could be observed
751 between CPF and CPF-CCNPs0.25 batches, especially at day 12 (6.78 *vs* 6.27 log CFU/g,
752 respectively). This may be ascribed to the antimicrobial effect of CIN by inhibiting amino acid
753 decarboxylase activity (Ouattara, Simard, Holley, Piette, & Bégin, 1997). This compound can
754 cross the cell wall and act intracellularly by the interaction of the CIN carbonyl group and proteins,
755 thus affecting the action of several proteins and enzymes (Wendakoon & Sakaguchi, 1995). At 16
756 days, all the batches were spoiled and the TVC increased beyond the acceptable limit (Fig. 10A).
757 Zarandona et al. (2021) also observed the TVC exceed 8 log CFU/g at 13 days during the chilled
758 storage of Atlantic horse mackerel.

759 The Gram-negative psychrotrophic bacteria counts (PTC) are the major group of microorganisms
760 responsible for spoilage of aerobically stored fresh fish at chilled temperatures (Sallam, 2007). The
761 initial PTC of the trout fillets was 3.24 log CFU/g at Day 0 (Fig. 10B). From 12 days onwards, all
762 batches showed evident signs of spoilage, reaching 8.16, 7.67, and 7.11 log CFU/g in control, CPF,

763 and CPF-CCNPs0.25 groups, respectively. However, the CPF-CCNPs0.25 wrapping resulted in
764 1.04 and 0.56 log CFU/g reductions in PTC of cold-stored fish ($p < 0.05$) on day 12 as compared
765 with the control and CPF-wrapped samples, respectively. The reduction of 1.8 log CFU/g of PTC
766 in tilapia fillets wrapped with plasma-treated LDPE coating containing 6% cinnamaldehyde was
767 reported by Loke, Chang, Hou, Cheng, and Hsieh (2021).

768 **4. Conclusions**

769 Herein active bionanocomposite films were developed by embedding CCNPs into CPF film
770 matrices. CCNPs were synthesized *via* the ionotropic gelation technique, and they presented a
771 spherical morphology with an apparent hydrodynamic diameter of 370.3 nm. The influences of the
772 NPs loaded with different amounts of CIN on the mechanical, barrier, structural, thermal,
773 morphological, and antimicrobial/antioxidant properties of CPF-CCNPs nanocomposite films
774 were discussed. A uniform distribution of the CCNPs was observed by SEM and their interactions
775 with polymer molecules were confirmed by ATR-FTIR and XRD spectra. The obtained
776 homogeneous bionanocomposite films showed better thermal stability and mechanical
777 performances. CCNPs-doped ternary films displayed a superior barrier capacity to the
778 transmission of light at 280 nm. Besides, nanoencapsulation technology was an effective way to
779 achieve sustained and controlled release of CIN from the films. Furthermore, the CPF films
780 incorporated with the CCNPs showed an improvement in their *in vitro* antibacterial activities
781 against four common food-borne pathogens (*S. aureus*, *L. monocytogenes*, *E. coli*, *and S.*
782 *enteritidis*). CCNP incorporation in the CPF polymeric systems also enhanced their antioxidant
783 capacity. Besides, the CPF-CCNPs nanocomposite films delayed the lipid oxidation and microbial
784 growth in rainbow trout fillets. The shelf-life of trout fillets was extended by wrapping with CPF-
785 based films from 8 days to 12 days (based on TVC and PTC) compared to the control. These

promising properties support the use of these CPF films reinforced with CCNPs as eco-friendly edible films for active packaging, where multifunctional bioactive systems are continuously necessary to protect and extend the shelf-life of foods.

Declaration of competing interest

The authors declared that they have no conflicts of interest to this work.

Acknowledgments

The study has been carried out with the financial support from Research Council of Tarbiat Modares University (IG-39804) and from Agencia Estatal de Investigación (AEI), through project AGL2017-84161.

References

Al-Tayyar, N. A., Youssef, A. M., & Al-Hindi, R. (2020a). Antimicrobial food packaging based on sustainable Bio-based materials for reducing foodborne Pathogens: A review. *Food Chemistry*, *310*, 125915.

Al-Tayyar, N. A., Youssef, A. M., & Al-Hindi, R. R. (2020b). Antimicrobial packaging efficiency of ZnO-SiO2 nanocomposites infused into PVA/CS film for enhancing the shelf life of food products. *Food Packaging and Shelf Life*, *25*, 100523.

Alves, V. L., Rico, B. P., Cruz, R. M., Vicente, A. A., Khmelinskii, I., & Vieira, M. C. (2018). Preparation and characterization of a chitosan film with grape seed extract-carvacrol microcapsules and its effect on the shelf-life of refrigerated Salmon (*Salmo salar*). *LWT*, *89*, 525-534.

806 ASTM. (2005). Standard test method for water vapor transmission of materials (E96-05). In
807 *Annual book of ASTM standards*. Philadelphia, PA: American Society for Testing Materials.
808 ASTM. (2009). Standard test method for tensile properties of thin plastic sheeting (D882-09). In
809 *Annual book of ASTM standards*. Philadelphia, PA: American Society for Testing Materials.
810 Bonilla, J., Fortunati, E. L. E. N. A., Atarés, L., Chiralt, A., & Kenny, J. M. (2014). Physical,
811 structural and antimicrobial properties of poly vinyl alcohol-chitosan biodegradable films.
812 *Food Hydrocolloids*, *35*, 463-470.
813 Burt, S. (2004). Essential oils: Their antibacterial properties and potential applications in foods –
814 A review. *International Journal of Food Microbiology*, 94, 223-253.
815 Castilho, L. R., Mitchell, D. A., & Freire, D. M. (2009). Production of polyhydroxyalkanoates
816 (PHAs) from waste materials and by-products by submerged and solid-state fermentation.
817 *Bioresource Technology*, *100*, 5996-6009.
818 Cazón, P., Vázquez, M., & Velazquez, G. (2018). Cellulose-glycerol-polyvinyl alcohol composite
819 films for food packaging: Evaluation of water adsorption, mechanical properties, light-barrier
820 properties and transparency. *Carbohydrate Polymers*, *195*, 432-443.
821 Chen, H., Hu, X., Chen, E., Wu, S., McClements, D. J., Liu, S., ... & Li, Y. (2016). Preparation,
822 characterization, and properties of chitosan films with cinnamaldehyde nanoemulsions. *Food*
823 *Hydrocolloids*, *61*, 662-671.
824 Chentir, I., Kchaou, H., Hamdi, M., Jridi, M., Li, S., Doumandji, A., & Nasri, M. (2019).
825 Biofunctional gelatin-based films incorporated with food grade phycocyanin extracted from
826 the Saharian cyanobacterium *Arthrospira* sp. *Food Hydrocolloids*, *89*, 715-725.
827 Coma, V., Martial-Gros, A., Garreau, S., Copinet, A., Salin, F., & Deschamps, A. (2002). Edible
828 antimicrobial films based on chitosan matrix. *Journal of Food Science*, 67, 1162-1169.

829 Cui, H., Surendhiran, D., Li, C., & Lin, L. (2020). Biodegradable zein active film containing
830 chitosan nanoparticle encapsulated with pomegranate peel extract for food packaging. *Food*
831 *Packaging and Shelf Life*, *24*, 100511.
832 de la Caba, K., Guerrero, P., Trung, T. S., Cruz-Romero, M., Kerry, J. P., Fluhr, J., ... & Newton,
833 R. (2019). From seafood waste to active seafood packaging: An emerging opportunity of the
834 circular economy. *Journal of Cleaner Production*, *208*, 86-98.
835 Fan, W., Yan, W., Xu, Z., & Ni, H. (2012). Formation mechanism of monodisperse, low molecular
836 weight chitosan nanoparticles by ionic gelation technique. *Colloids and Surfaces B:*
837 *Biointerfaces, 90*, 21–27.
838 Fang, Y., Tung, M. A., Britt, I. J., Yada, S., & Dalgleish, D. G. (2002). Tensile and barrier
839 properties of edible films made from whey proteins. *Journal of Food Science*, *67*, 188-193.
840 Farahmandghavi, F., Imani, M., & Hajiesmaeelian, F. (2019). Silicone matrices loaded with
841 levonorgestrel particles: Impact of the particle size on drug release. *Journal of Drug Delivery*
842 *Science and Technology*, *49*, 132-142.
843 Ghaderi, J., Hosseini, S. F., Keyvani, N., & Gómez-Guillén, M. C. (2019). Polymer blending
844 effects on the physicochemical and structural features of the chitosan/poly (vinyl alcohol)/fish
845 gelatin ternary biodegradable films. *Food Hydrocolloids*, *95*, 122-132.
846 Giteru, S. G., Ali, M. A., & Oey, I. (2019). Solvent strength and biopolymer blending effects on
847 physicochemical properties of zein-chitosan-polyvinyl alcohol composite films. *Food*
848 *Hydrocolloids*, *87*, 270-286.
849 Guerrero, P., Stefani, P. M., Ruseckaite, R. A., & de la Caba, K. (2011). Functional properties of
850 films based on soy protein isolate and gelatin processed by compression molding. Journal of
851 Food Engineering, 105, 65-72.

852 Hambleton, A., Fabra, M. J., Debeaufort, F., Dury-Brun, C., & Voilley, A. (2009). Interface and
853 aroma barrier properties of iota-carrageenan emulsion-based films used for encapsulation of
854 active food compounds. *Journal of Food Engineering*, *93*, 80-88.
855 Hosseini, S. F., & Gómez-Guillén, M. C. (2018). A state-of-the-art review on the elaboration of
856 fish gelatin as bioactive packaging: Special emphasis on nanotechnology-based approaches.
857 *Trends in Food Science & Technology*, *79*, 125-135.
858 Hosseini, S. F., Javidi, Z., & Rezaei, M. (2016). Efficient gas barrier properties of multilayer films
859 based on poly (lactic acid) and fish gelatin. *International Journal of Biological*
860 *Macromolecules*, *92*, 1205-1214.
861 Hosseini, S. F., Nahvi, Z., & Zandi, M. (2019). Antioxidant peptide-loaded electrospun
862 chitosan/poly (vinyl alcohol) nanofibrous mat intended for food biopackaging purposes. *Food*
863 *Hydrocolloids*, *89*, 637-648.
864 Hosseini, S. F., Ramezanzade, L., & McClements, D. J. (2021). Recent advances in
865 nanoencapsulation of hydrophobic marine bioactives: Bioavailability, safety, and sensory
866 attributes of nano-fortified functional foods. *Trends in Food Science & Technology*, *109*, 322-
867 339.
868 Hosseini, S. F., Rezaei, M., Zandi, M., & Farahmandghavi, F. (2015a). Bio-based composite edible
869 films containing *Origanum vulgare* L. essential oil. *Industrial Crops and products*, *67*, 403-
870 413.
871 Hosseini, S. F., Rezaei, M., Zandi, M., & Farahmandghavi, F. (2015b). Fabrication of
872 bionanocomposite films based on fish gelatin reinforced with chitosan nanoparticles. *Food*
873 *Hydrocolloids*, *44*, 172-182.

874 Hosseini, S. F., Rezaei, M., Zandi, M., & Farahmandghavi, F. (2016). Development of bioactive
875 fish gelatin/chitosan nanoparticles composite films with antimicrobial properties. *Food*
876 *Chemistry*, *194*, 1266-1274.
877 Hosseini, S. F., Soofi, M., & Rezaei, M. (2021). Enhanced physicochemical stability of ω-3
878 PUFAs concentrates-loaded nanoliposomes decorated by chitosan/gelatin blend coatings.
879 *Food Chemistry*, *345*, 128865.
880 Hosseini, S. F., Zandi, M., Rezaei, M., & Farahmandghavi, F. (2013). Two-step method for
881 encapsulation of oregano essential oil in chitosan NPs: Preparation, characterization and in
882 vitro release study. *Carbohydrate Polymers, 95*, 50-56.
883 Hyldgaard, M., Mygind, T., & Meyer, R. L. (2012). Essential oils in food preservation: mode of
884 action, synergies, and interactions with food matrix components. *Frontiers in Microbiology*,
885 *3*, 12.
886 Sallam, K. I. (2007). Antimicrobial and antioxidant effects of sodium acetate, sodium lactate, and
887 sodium citrate in refrigerated sliced salmon. *Food Control*, *18*(5), 566-575.
888 International commission on microbiological specifications for foods (ICMSF). (1986). Sampling
889 plans for fish and shellfish. In ICMSF (Ed.), *ICMSF, Microorganisms in foods. Sampling for*
890 *microbiological analysis: Principles and scientific applications* (2nd ed., pp. 181-196).
891 Canada: University of Toronto Press.
892 Javidi, Z., Hosseini, S. F., & Rezaei, M. (2016). Development of flexible bactericidal films based
893 on poly (lactic acid) and essential oil and its effectiveness to reduce microbial growth of
894 refrigerated rainbow trout. *LWT-Food Science and Technology*, *72*, 251-260.
895 Jouki, M., Yazdi, F. T., Mortazavi, S. A., Koocheki, A., & Khazaei, N. (2014). Effect of quince
896 seed mucilage edible films incorporated with oregano or thyme essential oil on shelf life

897 extension of refrigerated rainbow trout fillets. *International Journal of Food Microbiology*,
898 *174*, 88-97.
899 Kchaou, H., Jridi, M., Benbettaieb, N., Debeaufort, F., & Nasri, M. (2020). Bioactive films based
900 on cuttlefish (*Sepia officinalis*) skin gelatin incorporated with cuttlefish protein hydrolysates:
901 Physicochemical characterization and antioxidant properties. *Food Packaging and Shelf Life*,
902 *24*, 100477.
903 Ksouda, G., Sellimi, S., Merlier, F., Falcimaigne-Cordin, A., Thomasset, B., Nasri, M., & Hajji,
904 M. (2019). Composition, antibacterial and antioxidant activities of *Pimpinella saxifraga*
905 essential oil and application to cheese preservation as coating additive. *Food Chemistry*, *288*,
906 47-56.
907 Kuai, L., Liu, F., Ma, Y., Goff, H. D., & Zhong, F. (2020). Regulation of nano-encapsulated tea
908 polyphenol release from gelatin films with different Bloom values. *Food Hydrocolloids*, *108*,
909 106045.
910 Lian, H., Peng, Y., Shi, J., & Wang, Q. (2019). Effect of emulsifier hydrophilic-lipophilic balance
911 (HLB) on the release of thyme essential oil from chitosan films. *Food Hydrocolloids*, *97*,
912 105213.
913 Loke, X. J., Chang, C. K., Hou, C. Y., Cheng, K. C., & Hsieh, C. W. (2021). Plasma-treated
914 polyethylene coated with polysaccharide and protein containing cinnamaldehyde for active
915 packaging films and applications on tilapia (*Orechromis niloticus*) fillet preservation. *Food*
916 *Control*, *125*, 108016.
917 Martucci, J. F., & Ruseckaite, R. A. (2015). Biodegradation behavior of three-layer sheets based
918 on gelatin and poly (lactic acid) buried under indoor soil conditions. *Polymer Degradation*
919 *and Stability*, *116*, 36-44.

920 Mirzaei-Mohkam, A., Garavand, F., Dehnad, D., Keramat, J., & Nasirpour, A. (2020). Physical,
921 mechanical, thermal and structural characteristics of nanoencapsulated vitamin E loaded
922 carboxymethyl cellulose films. *Progress in Organic Coatings*, *138*, 105383.
923 Mo, X., Peng, X., Liang, X., Fang, S., Xie, H., Chen, J., & Meng, Y. (2021). Development of
924 antifungal gelatin-based nanocomposite films functionalized with natamycin-loaded
925 zein/casein nanoparticles. *Food Hydrocolloids*, *113*, 106506.
926 Mohajer, S., Rezaei, M., & Hosseini, S. F. (2017). Physico-chemical and microstructural
927 properties of fish gelatin/agar bio-based blend films. *Carbohydrate Polymers*, *157*, 784-793.
928 Narasagoudr, S. S., Hegde, V. G., Vanjeri, V. N., Chougale, R. B., & Masti, S. P. (2020). Ethyl
929 vanillin incorporated chitosan/poly (vinyl alcohol) active films for food packaging
930 applications. *Carbohydrate Polymers*, *236*, 116049.
931 Nilsuwan, K., Benjakul, S., & Prodpran, T. (2018). Properties and antioxidative activity of fish
932 gelatin-based film incorporated with epigallocatechin gallate. *Food Hydrocolloids*, *80*, 212-
933 221.
934 Norcino, L. B., Mendes, J. F., Natarelli, C. V. L., Manrich, A., Oliveira, J. E., & Mattoso, L. H. C.
935 (2020). Pectin films loaded with copaiba oil nanoemulsions for potential use as bio-based
936 active packaging. *Food Hydrocolloids*, *106*, 105862.
937 Ouattara, B., Simard, R. E., Holley, R. A., Piette, G. J. P., & Bégin, A. (1997). Antibacterial
938 activity of selected fatty acids and essential oils against six meat spoilage organisms.
939 *International Journal of Food Microbiology*, *37*(2-3), 155-162.
940 Pérez-Córdoba, L. J., Norton, I. T., Batchelor, H. K., Gkatzionis, K., Spyropoulos, F., & Sobral,
941 P. J. (2018). Physico-chemical, antimicrobial and antioxidant properties of gelatin-chitosan

942 based films loaded with nanoemulsions encapsulating active compounds. *Food*
943 *Hydrocolloids*, *79*, 544-559.
944 Pereira Jr, V. A., de Arruda, I. N. Q., & Stefani, R. (2015). Active chitosan/PVA films with
945 anthocyanins from Brassica oleraceae (Red Cabbage) as time-temperature indicators for
946 application in intelligent food packaging. *Food Hydrocolloids*, *43*, 180-188.
947 Raafat, D., Von Bargen, K., Haas, A., & Sahl, H. G. (2008). Insights into the mode of action of
948 chitosan as an antibacterial compound. *Applied and Environmental Microbiology*, *74*(12),
949 3764-3773.
950 Rhim, J. W., Park, H. M., & Ha, C. S. (2013). Bio-nanocomposites for food packaging
951 applications. *Progress in Polymer Science*, *38*(10-11), 1629-1652.
952 Sahariah, P., & Masson, M. (2017). Antimicrobial chitosan and chitosan derivatives: a review of
953 the structure–activity relationship. *Biomacromolecules*, *18*(11), 3846-3868.
954 Shahide, F. (1994). Seafood processing by-products. In F. Shahidi, & J. R. Botta (Eds.), *Seafoods*
955 *chemistry, processing, technology and quality* (pp. 320-334). Glasgow: Blackie Academic &
956 Professional.
957 Shreaz, S., Wani, W. A., Behbehani, J. M., Raja, V., Irshad, M., Karched, M., ... & Hun, L. T.
958 (2016). Cinnamaldehyde and its derivatives, a novel class of antifungal agents. *Fitoterapia*,
959 *112*, 116-131.
960 Silva, N. H., Vilela, C., Almeida, A., Marrucho, I. M., & Freire, C. S. (2018). Pullulan-based
961 nanocomposite films for functional food packaging: Exploiting lysozyme nanofibers as
962 antibacterial and antioxidant reinforcing additives. *Food Hydrocolloids*, *77*, 921-930.
963 Sun, J., Jiang, H., Li, M., Lu, Y., Du, Y., Tong, C., ... & Wu, C. (2020). Preparation and
964 characterization of multifunctional konjac glucomannan/carboxymethyl chitosan

965 biocomposite films incorporated with epigallocatechin gallate. *Food Hydrocolloids*, *105*,
966 105756.
967 Trinh, B. M., Chang, C. C., & Mekonnen, T. H. (2021). Facile fabrication of thermoplastic
968 starch/poly (lactic acid) multilayer films with superior gas and moisture barrier properties.
969 *Polymer*, *223*, 123679.
970 Uranga, J., Etxabide, A., Guerrero, P., & de la Caba, K. (2018). Development of active fish gelatin
971 films with anthocyanins by compression molding. *Food Hydrocolloids*, *84*, 313-320.
972 Vahedikia, N., Garavand, F., Tajeddin, B., Cacciotti, I., Jafari, S. M., Omidi, T., & Zahedi, Z.
973 (2019). Biodegradable zein film composites reinforced with chitosan nanoparticles and
974 cinnamon essential oil: Physical, mechanical, structural and antimicrobial attributes. *Colloids*
975 *and Surfaces B: Biointerfaces*, *177*, 25-32.
976 Vasile, F. E., Romero, A. M., Judis, M. A., & Mazzobre, M. F. (2016). Prosopis *alba* exudate gum
977 as excipient for improving fish oil stability in alginate-chitosan beads. *Food Chemistry*, *190*,
978 1093-1101.
979 Vilela, C., Kurek, M., Hayouka, Z., Röcker, B., Yildirim, S., Antunes, M. D. C., ... & Freire, C. S.
980 (2018). A concise guide to active agents for active food packaging. *Trends in Food Science &*
981 *Technology*, *80*, 212-222.
982 Volpe, M. G., Siano, F., Paolucci, M., Sacco, A., Sorrentino, A., Malinconico, M., & Varricchio,
983 E. (2015). Active edible coating effectiveness in shelf-life enhancement of trout
984 (*Oncorhynchusmykiss*) fillets. *LWT-Food Science and Technology*, *60*(1), 615-622.
985 Wang, H., Hao, L., Wang, P., Chen, M., Jiang, S., & Jiang, S. (2017). Release kinetics and
986 antibacterial activity of curcumin loaded zein fibers. *Food Hydrocolloids*, *63*, 437-446.

987 Wang, L. F., & Rhim, J. W. (2015). Preparation and application of agar/alginate/collagen ternary
988 blend functional food packaging films. *International Journal of Biological Macromolecules*,
989 *80*, 460-468.
990 Wang, Y., Zhang, R., Qin, W., Dai, J., Zhang, Q., Lee, K., & Liu, Y. (2020). Physicochemical
991 properties of gelatin films containing tea polyphenol-loaded chitosan nanoparticles generated
992 by electrospray. *Materials & Design*, *185*, 108277.
993 Wendakoon, C. N., & Sakaguchi, M. (1995). Inhibition of amino acid decarboxylase activity of
994 Enterobacter aerogenes by active components in spices. *Journal of Food Protection*, *58*(3),
995 280-283.
996 Wu, C., Li, Y., Du, Y., Wang, L., Tong, C., Hu, Y., ... & Yan, Z. (2019). Preparation and
997 characterization of konjac glucomannan-based bionanocomposite film for active food
998 packaging. *Food Hydrocolloids*, *89*, 682-690.
999 Wu, C., Li, Y., Sun, J., Lu, Y., Tong, C., Wang, L., ... & Pang, J. (2020). Novel konjac
1000 glucomannan films with oxidized chitin nanocrystals immobilized red cabbage anthocyanins
1001 for intelligent food packaging. *Food Hydrocolloids*, *98*, 105245.
1002 Wu, J., Sun, Q., Huang, H., Duan, Y., Xiao, G., & Le, T. (2019). Enhanced physico-mechanical,
1003 barrier and antifungal properties of soy protein isolate film by incorporating both plant-
1004 sourced cinnamaldehyde and facile synthesized zinc oxide nanosheets. *Colloids and Surfaces*
1005 *B: Biointerfaces*, *180*, 31-38.
1006 Wu, Y., Ying, Y., Liu, Y., Zhang, H., & Huang, J. (2018). Preparation of chitosan/poly vinyl
1007 alcohol films and their inhibition of biofilm formation against *Pseudomonas aeruginosa*
1008 PAO1. *International Journal of Biological Macromolecules*, *118*, 2131-2137.

1009 Wu, C., Zhu, Y., Wu, T., Wang, L., Yuan, Y. I., Chen, J., ... & Pang, J. (2019). Enhanced functional
1010 properties of biopolymer film incorporated with curcurmin-loaded mesoporous silica
1011 nanoparticles for food packaging. *Food Chemistry*, *288*, 139-145.
1012 Xue, F., Gu, Y., Wang, Y., Li, C., & Adhikari, B. (2019). Encapsulation of essential oil in emulsion
1013 based edible films prepared by soy protein isolate-gum acacia conjugates. *Food*
1014 *Hydrocolloids*, *96*, 178-189.
1015 Yagiz, Y., Kristinsson, H. G., Balaban, M. O., & Marshall, M. R. (2007). Effect of high pressure
1016 treatment on the quality of rainbow trout (*Oncorhynchus mykiss*) and mahi mahi (*Coryphaena*
1017 *hippurus*). *Journal of Food Science*, *72*(9), 509-515.
1018 Yıldırım, A., Mavi, A., & Kara, A. A. (2001). Determination of antioxidant and antimicrobial
1019 activities of Rumex crispus L. extracts. *Journal of Agricultural and Food Chemistry*, *49*(8),
1020 4083-4089.
1021 Yuan, Y., Zhang, X., Pan, Z., Xue, Q., Wu, Y., Li, Y., ... & Li, L. (2021). Improving the properties
1022 of chitosan films by incorporating shellac nanoparticles. *Food Hydrocolloids*, *110*, 106164.
1023 Zarandona, I., López-Caballero, M. E., Montero, M. P., Guerrero, P., de la Caba, K., & Gómez-
1024 Guillén, M. C. (2021). Horse mackerel (*Trachurus trachurus*) fillets biopreservation by using
1025 gallic acid and chitosan coatings. *Food Control*, *120*, 107511.
1026 Zhao, R., Guan, W., Zheng, P., Tian, F., Zhang, Z., Sun, Z., & Cai, L. (2021). Development of
1027 edible composite film based on chitosan nanoparticles and their application in packaging of
1028 fresh red sea bream fillets. *Food Control*, 108545.
1029

Figure captions

Fig. 1. (A) SEM image, (B) TEM image, (C) size distribution, and (D) ζ-potential of CCNPs.

Fig. 2. (A) Typical stress-strain and (B) light-transmittance curves of the CPF films incorporated with different amounts of CCNPs.

Fig. 3. (A) ATR-FTIR spectra, (B) XRD patterns, and (C) DSC thermograms of (a) control CPF film, and CPF films incorporated with (b) blank NPs (CPF-CCNPs0) and (c) the highest amount of CIN-loaded NPs (CPF-CCNPs0.25).

Fig. 4. (A) TGA and (B) DTG thermograms of (a) control CPF film, and CPF films incorporated with (b) blank NPs (CPF-CCNPs0) and (c) the highest amount of CIN-loaded NPs (CPF-CCNPs0.25).

Fig. 5. SEM micrographs of the surface and cross-section of (A, a) control CPF film, and CPF films incorporated with (B, b) blank NPs (CPF-CCNPs0) and (C, c) the highest amount of CIN-loaded NPs (CPF-CCNPs0.25).

Fig. 6. 3D AFM images together with the corresponding height profiles of (a) control CPF film, and CPF films incorporated with (b) blank NPs (CPF-CCNPs0) and (c) the highest amount of CIN-loaded NPs (CPF-CCNPs0.25).

Fig. 7. Cumulative release of CIN from CPF-CCNPs films at different amounts of CIN-loaded NPs. Error bars indicate standard deviation.

Fig. 8. Changes in (A) pH and (B) TBARS values of rainbow trout fillets stored at 4 °C for 16 days. Error bars indicate standard deviation.

Fig. 9. Changes in color parameters (CIELab) of rainbow trout fillets stored at 4 °C for 16 days: (A) L* (lightness), (B) a* (redness/greenness), and (C) b* (yellowness/blueness) values. Error bars indicate standard deviation.

Fig. 10. Changes in (A) total viable counts (TVC) and (B) psychrotrophic counts (PTC) of rainbow trout fillets stored at 4 °C for 16 days. Error bars indicate standard deviation.

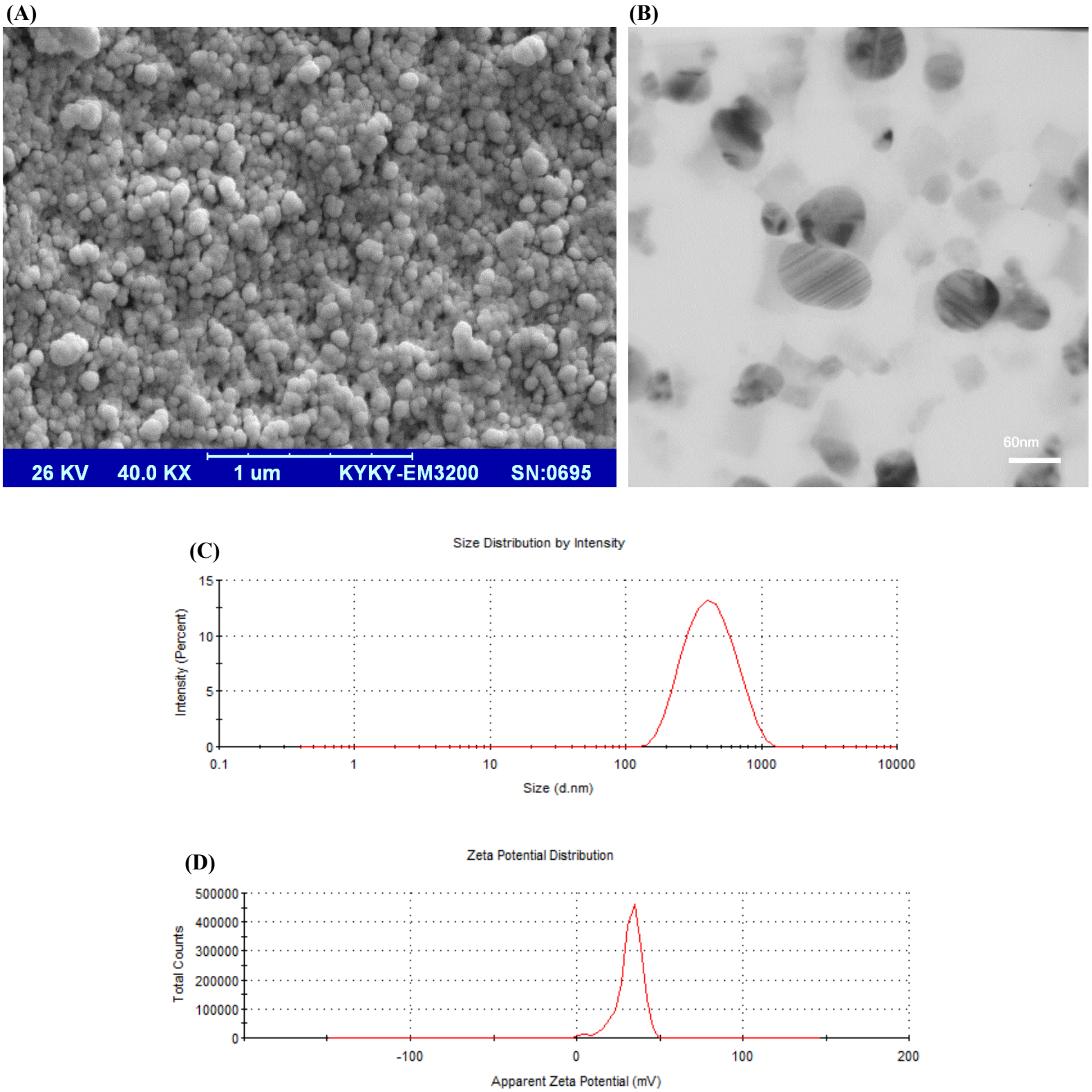
(A)
26 KV 40.0 KX 1 um KYKY-EM3200 SN:0695
(B)
60nm
(C)
Size Distribution by Intensity
Intensity (Percent)
15
10
5
0
0.1
1
10
100
1000
10000
Size (d.nm)
(D)
Zeta Potential Distribution
Total Counts
500000
400000
300000
200000
100000
0
-100
0
100
200
Apparent Zeta Potential (mV)

Fig. 1.

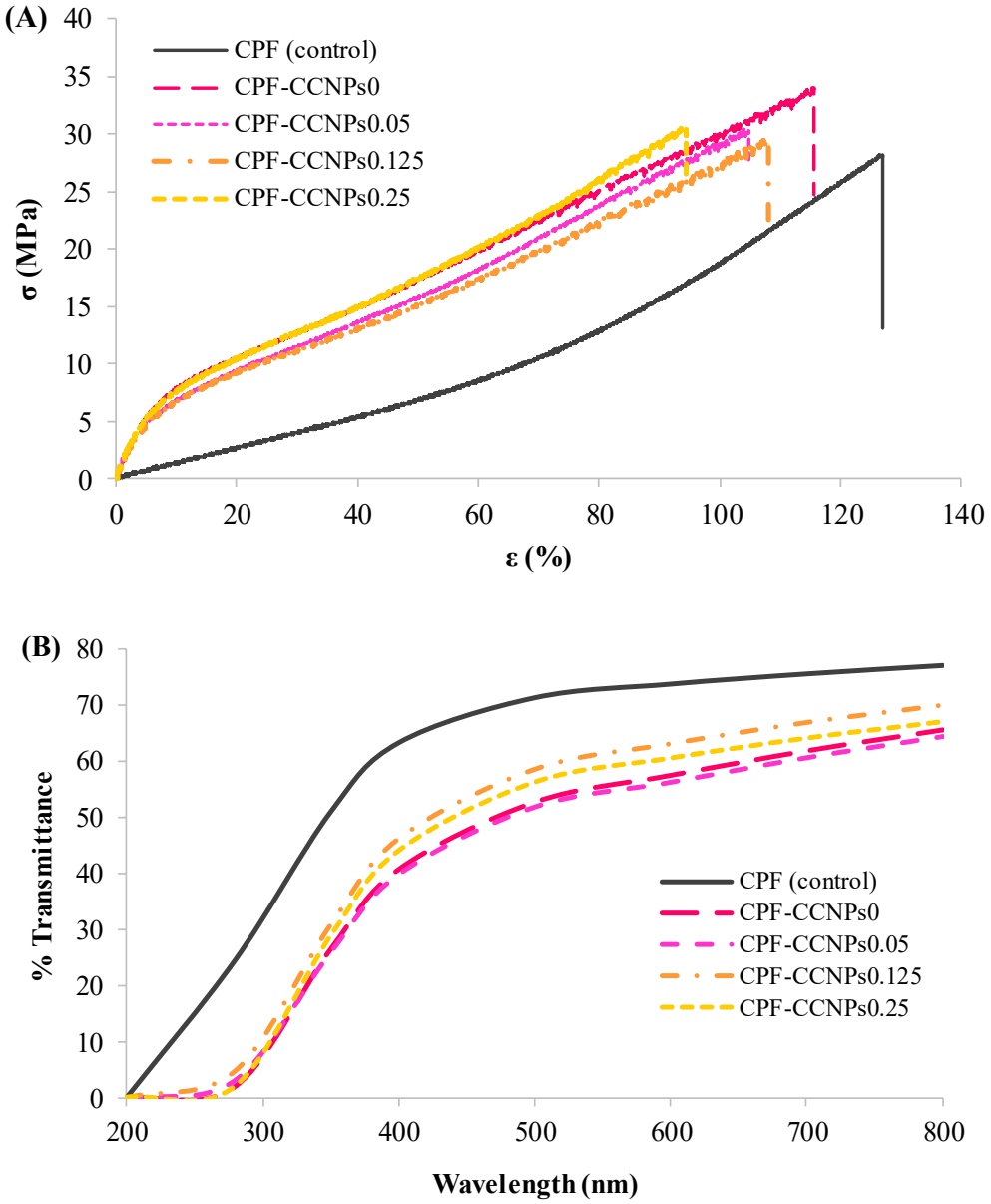
(A)
σ (MPa)
ε (%)
CPF (control)
CPF-CCNPs0
CPF-CCNPs0.05
CPF-CCNPs0.125
CPF-CCNPs0.25
(B)
% Transmittance
Wavelength (nm)
CPF (control)
CPF-CCNPs0
CPF-CCNPs0.05
CPF-CCNPs0.125
CPF-CCNPs0.25

Fig. 2.

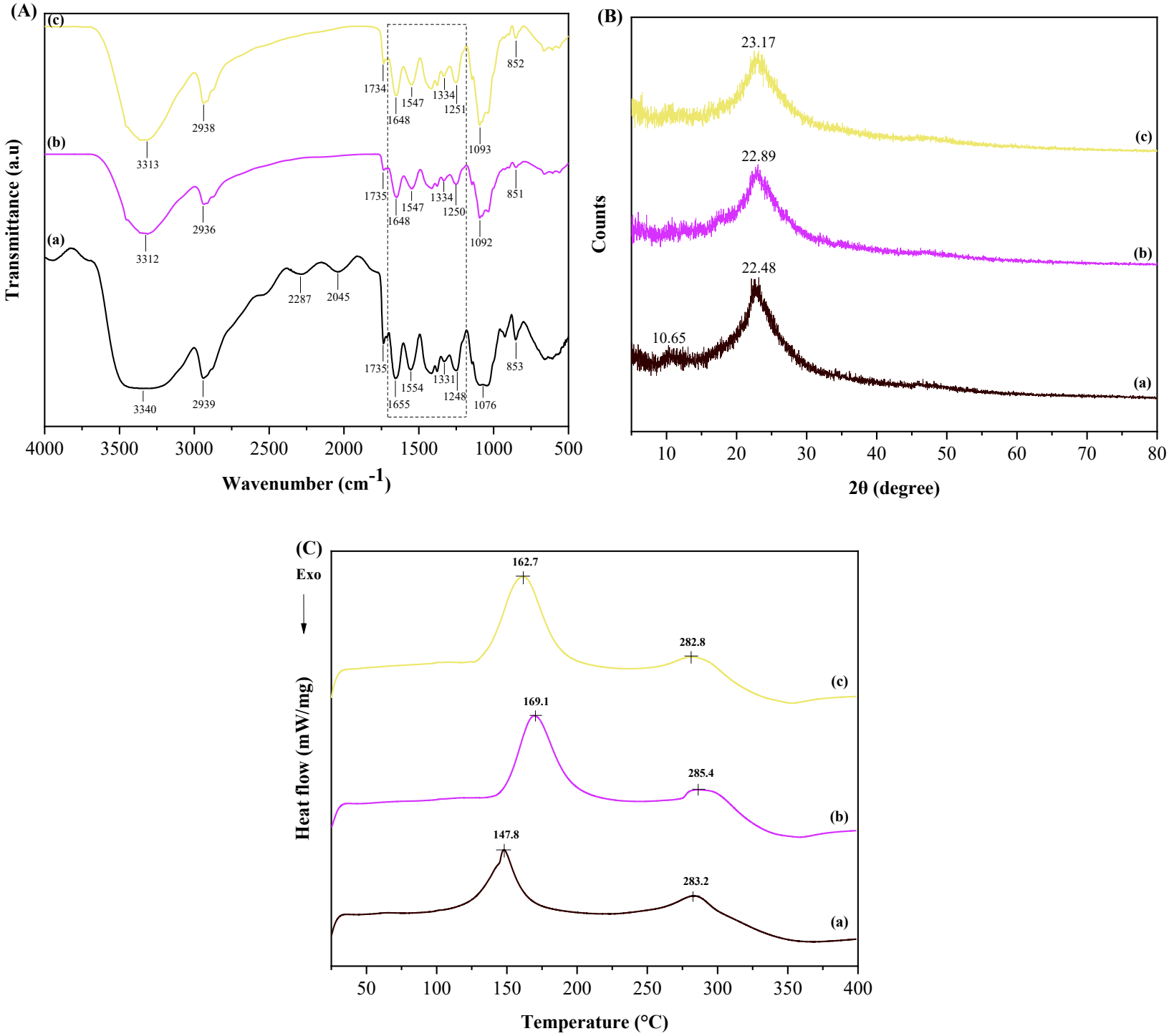
(A)
(c)
(b)
(a)
Transmittance (a.u)
Wavenumber (cm-1)
4000
3500
3000
2500
2000
1500
1000
500
3313
2938
1734
1648
1547
1334
1251
1093
852
3312
2936
1735
1648
1547
1334
1250
1092
851
3340
2939
2287
2045
1735
1655
1554
1331
1248
1076
853
(B)
Counts
23.17
22.89
22.48
10.65
(c)
(b)
(a)
10
20
30
40
50
60
70
80
2θ (degree)
(C)
Exo
Heat flow (mW/mg)
162.7
282.8
169.1
285.4
147.8
283.2
(c)
(b)
(a)
50
100
150
200
250
300
350
400
Temperature (°C)

Fig. 3.

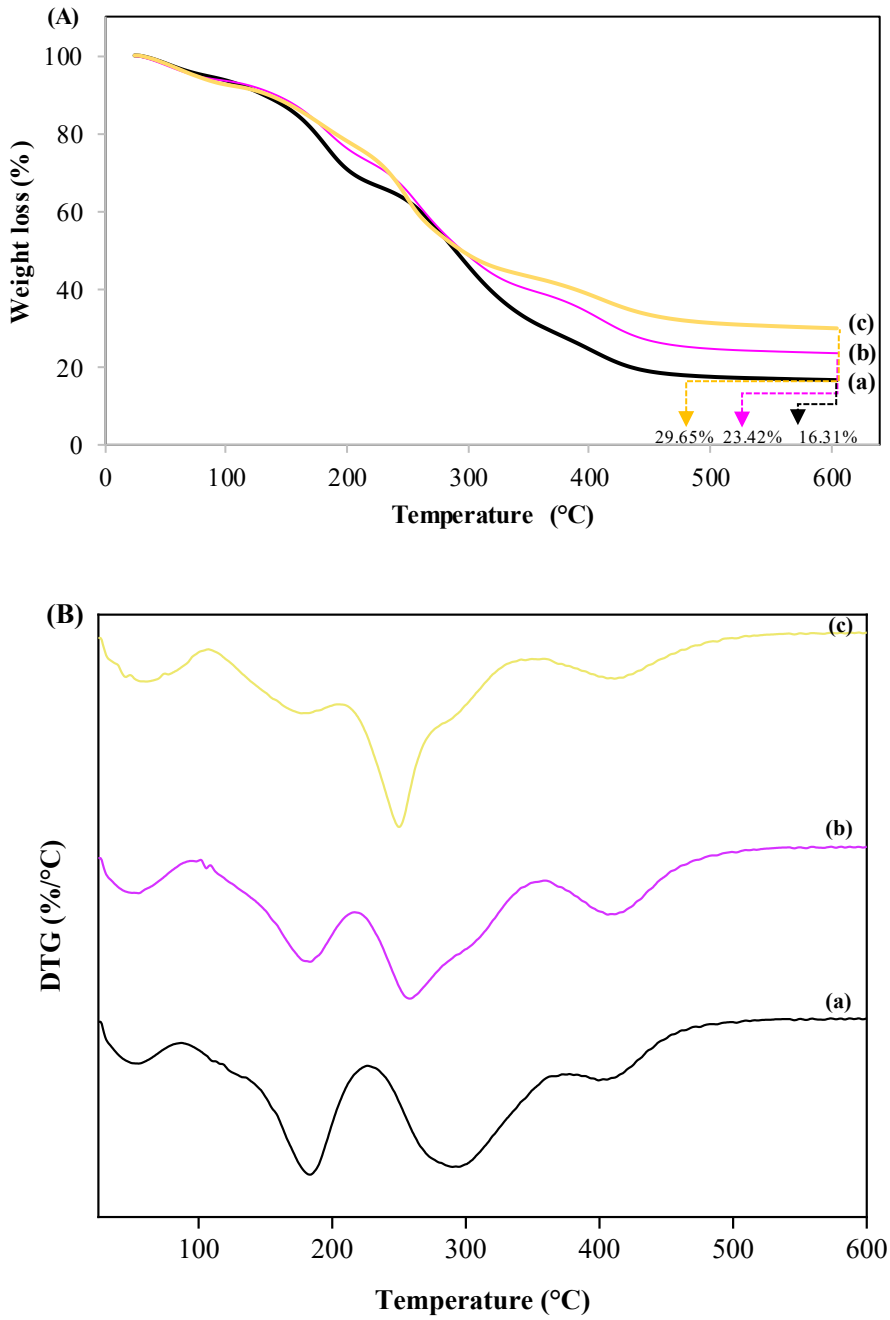
(A)
Weight loss (%)
100
80
60
40
20
0
0
100
200
300
400
500
600
Temperature (°C)
(c)
(b)
(a)
29.65%
23.42%
16.31%
(B)
DTG (%/°C)
(c)
(b)
(a)
100
200
300
400
500
600
Temperature (°C)

Fig. 4.

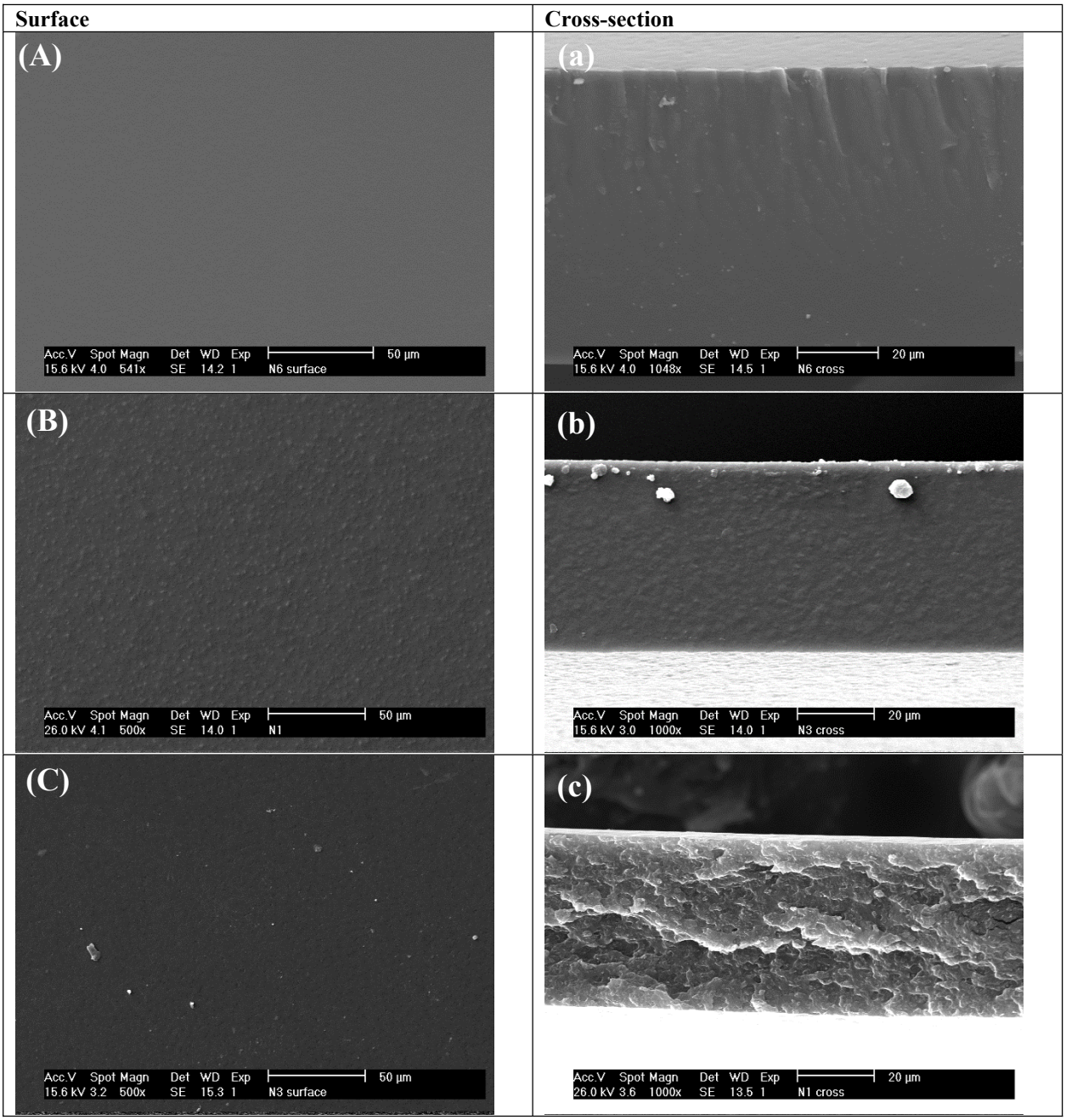
Surface
Cross-section
(A)
Acc.V Spot Magn Det WD Exp 50 µm
15.6 kV 4.0 541x SE 14.2 1 N6 surface
(a)
Acc.V Spot Magn Det WD Exp 20 µm
15.6 kV 4.0 1048x SE 14.5 1 N6 cross
(B)
Acc.V Spot Magn Det WD Exp 50 µm
26.0 kV 4.1 500x SE 14.0 1 N1
(b)
Acc.V Spot Magn Det WD Exp 20 µm
15.6 kV 3.0 1000x SE 14.0 1 N3 cross
(C)
Acc.V Spot Magn Det WD Exp 50 µm
15.6 kV 3.2 500x SE 15.3 1 N3 surface
(c)
Acc.V Spot Magn Det WD Exp 20 µm
26.0 kV 3.6 1000x SE 13.5 1 N1 cross

Fig. 5.

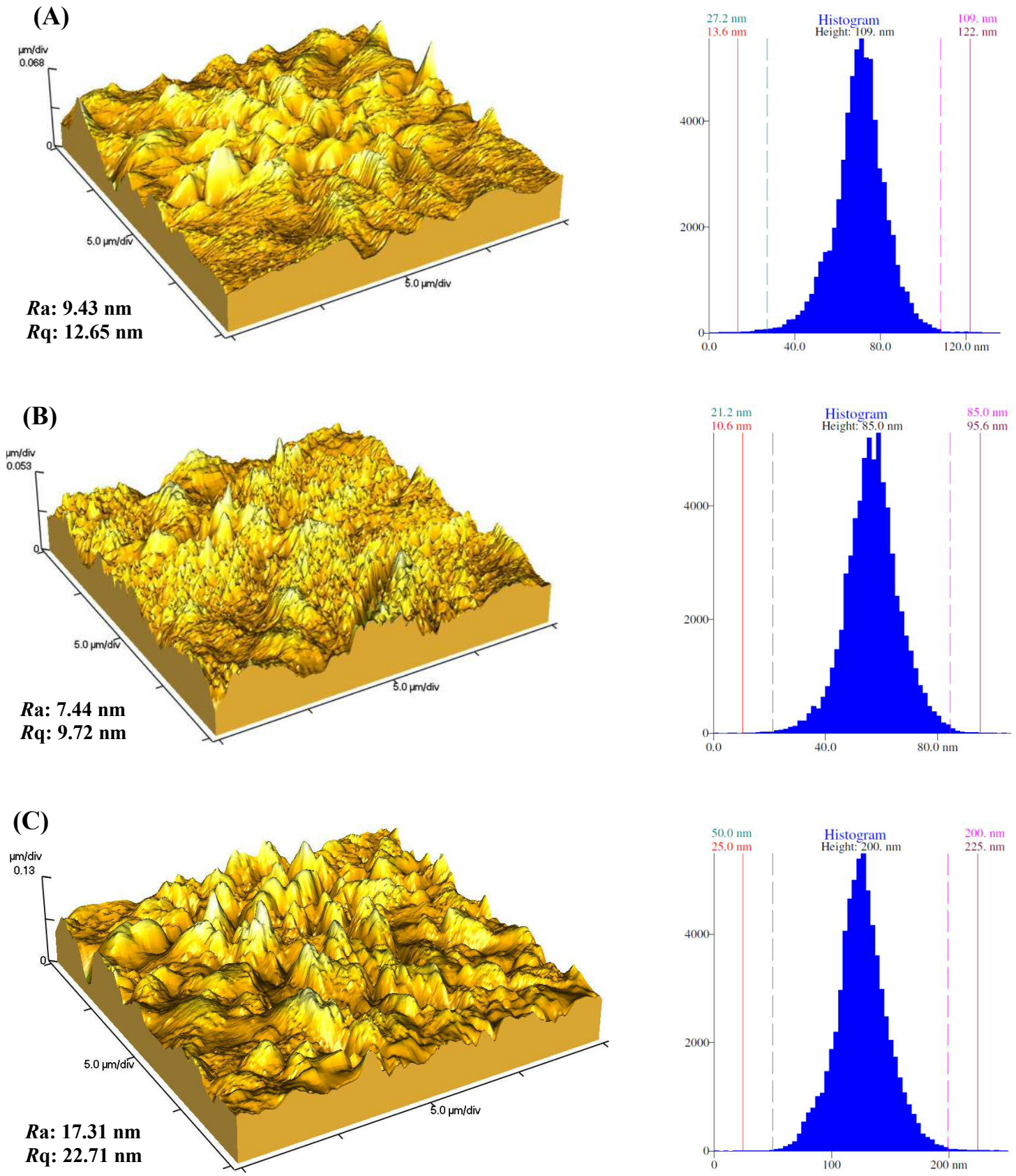
(A)
µm/div
0.068
0
5.0 µm/div
5.0 µm/div
Ra: 9.43 nm
Rq: 12.65 nm
27.2 nm
13.6 nm
Histogram
Height: 109. nm
109. nm
122. nm
4000
2000
0
0.0
40.0
80.0
120.0 nm
(B)
µm/div
0.053
0
5.0 µm/div
5.0 µm/div
Ra: 7.44 nm
Rq: 9.72 nm
21.2 nm
10.6 nm
Histogram
Height: 85.0 nm
85.0 nm
95.6 nm
4000
2000
0
0.0
40.0
80.0 nm
(C)
µm/div
0.13
0
5.0 µm/div
5.0 µm/div
Ra: 17.31 nm
Rq: 22.71 nm
50.0 nm
25.0 nm
Histogram
Height: 200. nm
200. nm
225. nm
4000
2000
0
0
100
200 nm

Fig. 6.

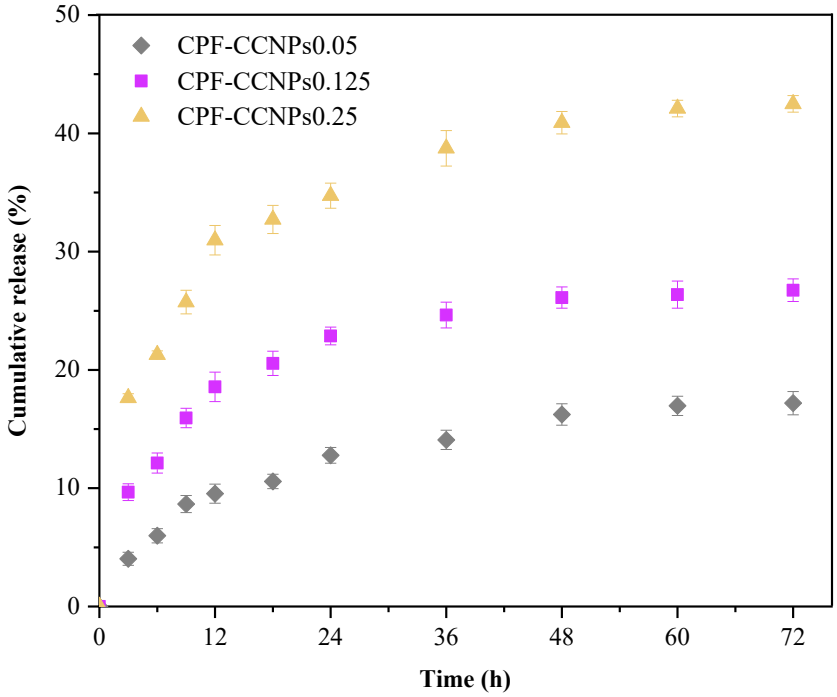
CPF-CCNPs0.05
CPF-CCNPs0.125
CPF-CCNPs0.25
Cumulative release (%)
Time (h)
0
10
20
30
40
50
0
12
24
36
48
60
72

Fig. 7.

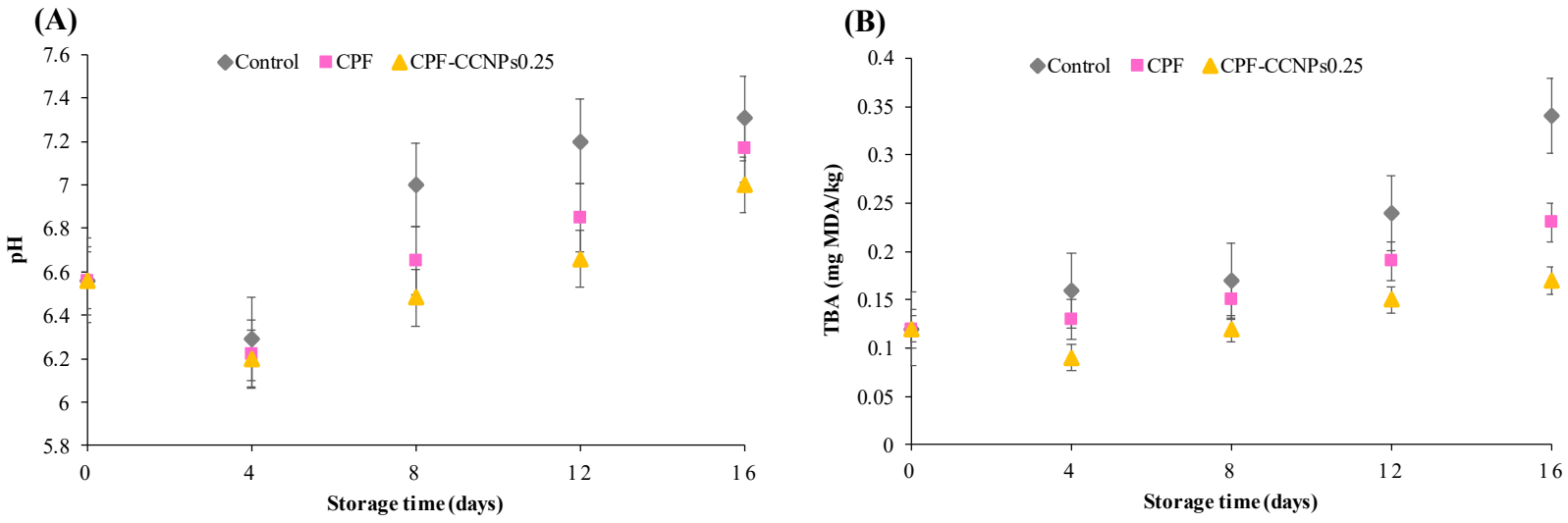
(A)
Control
CPF
CPF-CCNPs0.25
pH
7.6
7.4
7.2
7
6.8
6.6
6.4
6.2
6
5.8
0
4
8
12
16
Storage time (days)
(B)
Control
CPF
CPF-CCNPs0.25
TBA (mg MDA/kg)
0.4
0.35
0.3
0.25
0.2
0.15
0.1
0.05
0
0
4
8
12
16
Storage time (days)

Fig. 8.

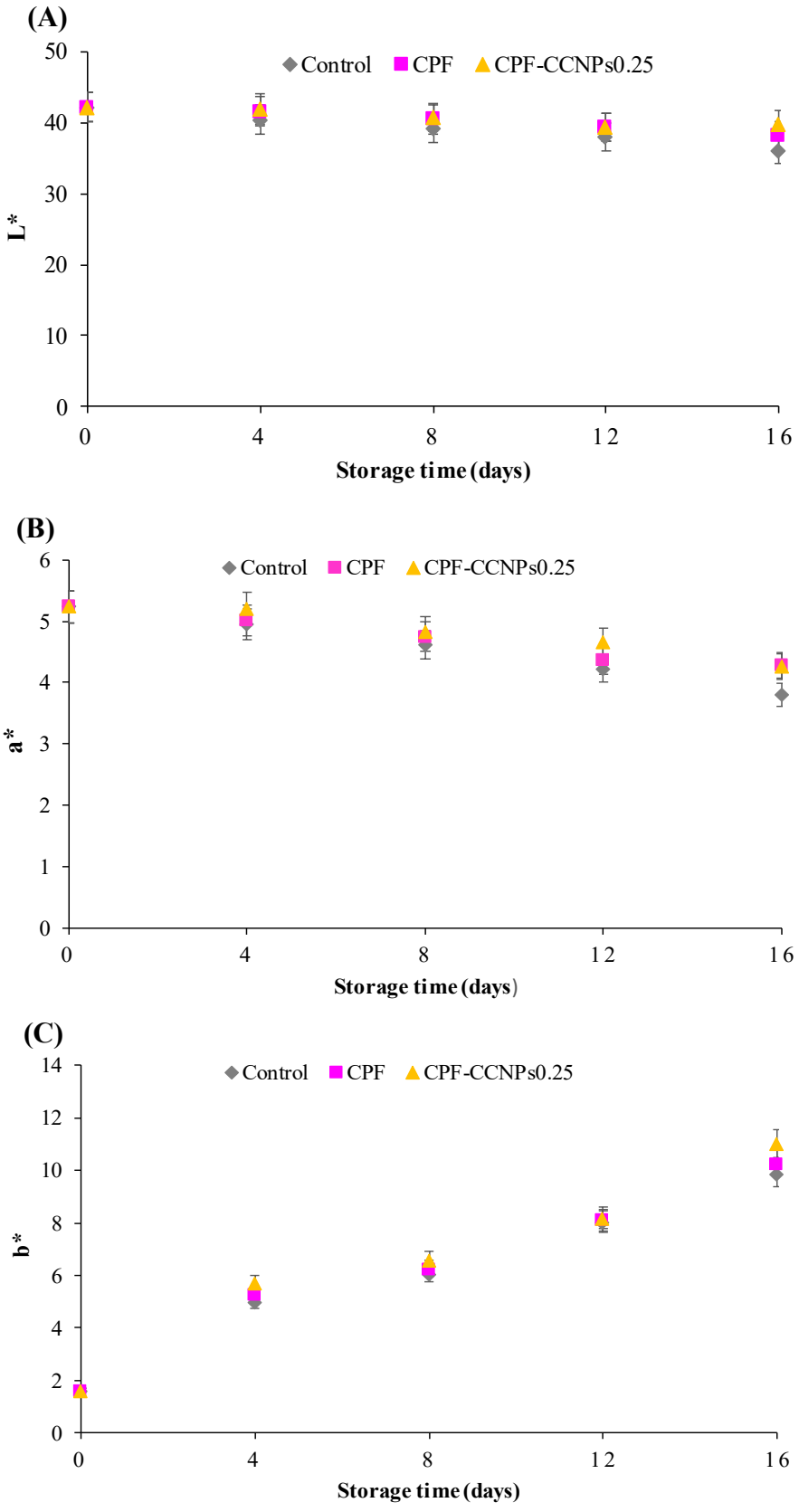
(A)
Control
CPF
CPF-CCNPs0.25
L*
Storage time (days)
(B)
Control
CPF
CPF-CCNPs0.25
a*
Storage time (days)
(C)
Control
CPF
CPF-CCNPs0.25
b*
Storage time (days)

Fig. 9.

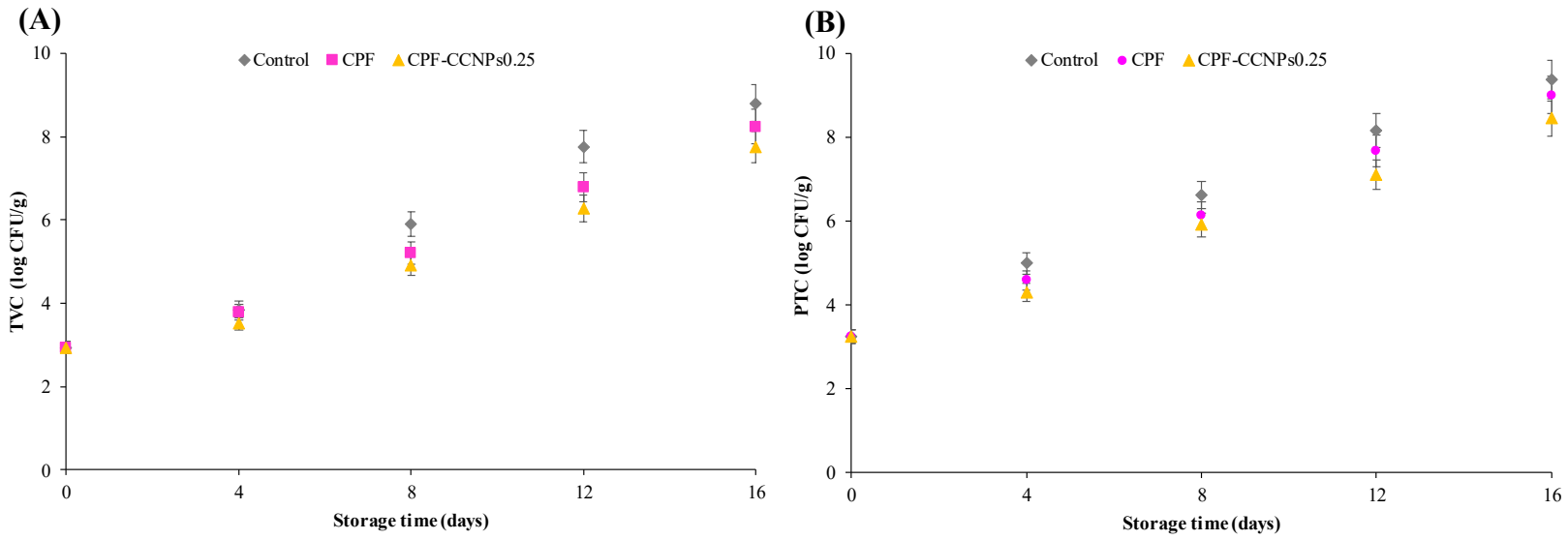
(A)
Control
CPF
CPF-CCNPs0.25
TVC (log CFU/g)
Storage time (days)
(B)
Control
CPF
CPF-CCNPs0.25
PTC (log CFU/g)
Storage time (days)

Fig. 10.

Table Click here to access/download;Table;Tables.docx

Table 1

Thickness, tensile strength (TS), elongation-at-break (EAB), water vapor permeability (WVP), and water contact angle (CA) of the CPF films incorporated with different amounts of CCNPs.

Samples	Thickness (μm)	TS (MPa)	EAB (%)	WVP (g mm/kPa h m^2)	WCA (°)			
					$t = 0$ s	Images	$t = 10$ s	Images
CPF (control)	0.046 ± 0.001^{a}	28.33 ± 2.17^{a}	128.39 ± 11.32^{a}	0.785 ± 0.053^{ab}	73.85 ± 2.76^{a}	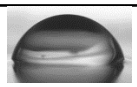	76.06 ± 2.00^{ab}	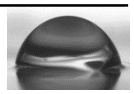
CPF-CCNPs0	0.047 ± 0.001^{a}	33.00 ± 1.28^{b}	119.31 ± 13.23^{a}	0.692 ± 0.049^{a}	74.00 ± 0.98^{a}	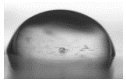	74.80 ± 0.56^{a}	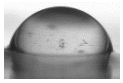
CPF-CCNPs0.05	0.049 ± 0.002^{b}	32.03 ± 1.21^{b}	112.46 ± 6.13^{ab}	0.670 ± 0.084^{a}	74.13 ± 1.50^{a}	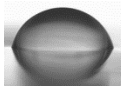	74.90 ± 0.42^{a}	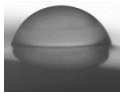
CPF-CCNPs0.125	0.050 ± 0.001^{bc}	31.94 ± 1.43^{b}	98.21 ± 4.81^{bc}	0.822 ± 0.007^{b}	73.65 ± 0.35^{a}	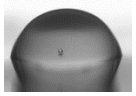	78.93 ± 2.45^{b}	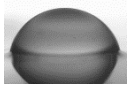
CPF-CCNPs0.25	0.052 ± 0.002^{c}	28.90 ± 1.86^{a}	90.82 ± 5.25^{c}	0.836 ± 0.008^{b}	73.46 ± 2.44^{a}	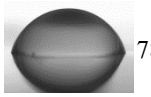	78.16 ± 1.96^{ab}	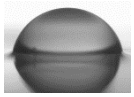

Values are expressed as the mean ± standard deviation. Superscripts bearing different lower case letters in the same column indicate significant differences ($p < 0.05$).

Table 2

Color parameters (CIELab) and total color difference (ΔE), and opacity values of the CPF films incorporated with different amounts of CCNPs.

Samples	Color parameters				Opacity (UA/mm)
	L^*	a^*	b^*	ΔE	
CPF (control)	28.11 ± 0.07[a]	3.64 ± 0.05[a]	7.71 ± 0.10[a]	67.04 ± 0.07[a]	1.37 ± 0.09[a]
CPF-CCNPs0	27.09 ± 0.67[ab]	4.52 ± 0.15[b]	10.23 ± 0.23[b]	68.43 ± 0.62[b]	3.08 ± 0.11[b]
CPF-CCNPs0.05	26.49 ± 0.60[b]	4.35 ± 0.15[b]	9.34 ± 0.21[c]	68.88 ± 0.63[b]	3.15 ± 0.10[b]
CPF-CCNPs0.125	26.34 ± 1.12[b]	4.45 ± 0.12[b]	9.28 ± 0.39[c]	69.04 ± 1.14[b]	3.45 ± 0.08[c]
CPF-CCNPs0.25	26.14 ± 0.86[b]	4.09 ± 0.12[c]	9.52 ± 0.03[c]	69.24 ± 0.85[b]	3.68 ± 0.12[d]

Values are expressed as the mean ± standard deviation. Superscripts bearing different lower case letters in the same column indicate significant differences ($p < 0.05$).

Table 3

Antimicrobial and antioxidant activity of the CPF films incorporated with different amounts of CCNPs.

Samples	Inhibition zone (mm)				DPPH scavenging (%)	Reducing power ($OD_{700\ nm}$)
	S. aureus	*L. monocytogenes*	*S. enteritidis*	*E. coli*		
CPF (control)	0.00^{a}	0.00^{a}	0.00 ± 0.00^{a}	0.00^{a}	11.11 ± 0.83^{a}	0.084 ± 0.011^{a}
CPF-CCNPs0	0.00^{a}	0.00^{a}	0.00 ± 0.00^{a}	0.00^{a}	13.16 ± 3.24^{ab}	0.098 ± 0.001^{b}
CPF-CCNPs0.05	0.00^{a}	0.00^{a}	0.00 ± 0.00^{a}	0.00^{a}	13.64 ± 2.22^{ab}	0.106 ± 0.007^{bc}
CPF-CCNPs0.125	5.25 ± 0.77^{b}	5.60 ± 0.70^{b}	4.73 ± 0.47^{b}	3.36 ± 0.40^{b}	15.22 ± 3.07^{ab}	0.122 ± 0.009^{cd}
CPF-CCNPs0.25	6.00 ± 1.13^{b}	6.60 ± 1.20^{b}	5.90 ± 0.56^{c}	4.94 ± 0.34^{c}	16.43 ± 1.02^{b}	0.128 ± 0.002^{d}

Values are expressed as the mean ± standard deviation. Superscripts bearing different lower case letters in the same column indicate significant differences ($p < 0.05$).